*sustainability*

MDPI

*Article*

# Tannin-Based Insulation Foams: The Effect of the Substitution of Formalin with Glutaraldehyde

**Alessandra Ranesi [1,*], Paulina Faria [1,*], António Santos Silva [2] and Ana Luísa Fernando [3,4]**

[1] CERIS—Civil Engineering Research and Innovation for Sustainability, NOVA School of Science and Technology, NOVA University Lisbon, 2829-516 Caparica, Portugal
[2] Materials Department, National Laboratory for Civil Engineering, 1700-066 Lisbon, Portugal; s.silva@lnec.pt
[3] MEtRICs—Mechanical Engineering and Resources Sustainability Center, Departamento de Química, NOVA School of Science and Technology, NOVA University Lisbon, 2829-516 Caparica, Portugal; ala@fct.unl.pt
[4] LAQV-REQUIMTE, Departamento de Química, NOVA School of Science and Technology, NOVA University Lisbon, 2829-516 Caparica, Portugal
* Correspondence: a.ranesi@fct.unl.pt (A.R.); paulina.faria@fct.unl.pt (P.F.)

## Abstract

This study investigates the potential of tannin-based foams as sustainable thermal insulations, analysing how the type and ratio of crosslinker (formalin and glutaraldehyde) and the addition of natural fibres can affect their mechanical, moisture-related, hygrothermal and fire-related performance, in comparison to commercial polystyrene. Formulations prepared with a single crosslinking agent (formalin or glutaraldehyde) exhibited lower densities (50.81 kg/m$^3$ and 53.37 kg/m$^3$, respectively), whereas the combined use of both crosslinkers resulted in higher apparent densities, with the maximum values observed for the intermediate substitution levels. The 100% glutaraldehyde foams showed higher compressive and flexural strengths than foams with 100% formalin (79 vs. 77 kPa and 160 vs. 120 kPa, respectively). A non-linear relationship between crosslinker composition and mechanical performance was observed, as the hybrid formulations did not consistently display intermediate properties. The 50/50 formulation showed about 40–46% lower compressive strength than the other foams; the loss appeared to be recovered by the addition of fibres (with Cs passing from 43 to 76 kPa). These results indicate that fibre addition is beneficial when higher stiffness is required, such as for sandwich panels or impact-resistant components. The substitution of F with G at 75% introduced an increase in the flexural strength of approx. 43% and the highest recovery after deformation (after 24 h, 75% of the original thickness). Tannin foams show high water vapour permeability (1.04–1.17 × $10^{-10}$ kg/(m·s·Pa)), potentially favouring moisture transport in permeable walls, although their sensitivity to liquid water highlights the need for protective layers in moisture-exposed applications. Thermal conductivity remains within the expected range for bio-based insulations (0.043–0.054 W/(m·K)). Tannin foams also show no flaming droplets or released smoke when ignited and high char formation in preliminary tests, reinforcing their potential as safer alternatives to petroleum-based insulations. The substitution of formalin with glutaraldehyde did not show any difference in heavy-metal-related toxicity. Overall, tannin-based foams represent a promising class of bio-insulations for protected sandwich panels, suitable for the implementation of low-carbon and circular construction strategies.

**Keywords:** eco-friendly insulation; bark tannin; mechanical characterisation; water- and fire-related performance; hygrothermal behaviour

Check for updates

Academic Editors: Francesco Tajani, Pierluigi Morano, Felicia Di Liddo and Paola Amoruso

Received: 27 August 2026
Revised: 14 October 2026
Accepted: 15 October 2026
Published: 22 October 2026

**Copyright:** © 2026 by the authors. Licensee MDPI, Basel, Switzerland. This article is an open access article distributed under the terms and conditions of the Creative Commons Attribution (CC BY) license.

## 1. Introduction

The building sector is responsible for a substantial share of global energy consumption and greenhouse gas emissions, making the improvement of building envelope performance a priority for climate mitigation strategies. In Europe (EU), approximately 75% of the existing building stock remains energy-inefficient and requires renovation, driving a growing demand for thermal insulation materials [1]. However, conventional insulation products such as mineral wool (MW), expanded and extruded polystyrene (EPS, XPS) and polyurethane (PU) require high thermal treatments, are predominantly derived from non-renewable resources and/or rely heavily on primary raw materials. In 2016, insulation manufacturing in the EU-28 required about 6.4 M tonnes of resources, 78% of which originated from raw materials [2]. Even under closed-loop recycling scenarios, reductions in primary material demand remain limited, highlighting the need for complementary strategies that include the development of renewable, bio-based alternatives.

Bio-based insulations have, therefore, gained increasing attention as sustainable solutions capable of reducing environmental impacts while providing competitive thermal performance. Derived partially or entirely from animal fibres or plant-based biomass, these insulations include bio-based polyurethane (synthesised using bio-based polyols), cellulose and polylactic acids [3]. Their intrinsic properties, low embodied carbon, biodegradability and the ability to store biogenic carbon position them as promising candidates for circular construction models [4,5]. Bio-based insulations can be classified into several categories, depending on the nature of the matrix and reinforcement phases (commonly fibres), from the more generic bio-based insulations to the more specific bio-polymer composites or, if bio-reinforced, hybrid bio-composites or green composites [5]. According to Cosentino et al. [6], the thermal conductivity of bio-based insulations is strongly influenced by their density and is competitive with that of conventional fossil-fuel-based insulations. The same researchers also reported that bio-based insulations generally show high moisture diffusivity (preserving the moisture transfer of building envelopes) and release less smoke during combustion compared to expanded polystyrene. Their mechanical performance, however, is more dependent on composition, with literature showing a wide variability in compressive strength values, ranging from 3.13 MPa for clay–wheat straw composite to 0.024 MPa for corn husk composite [6].

Despite their advantages, bio-based insulations still face challenges related to variability in composition, moisture sensitivity and limited standardisation. Mort et al. [3] highlight significant knowledge gaps regarding the relationships between structure, processing and thermal performance, with available datasets often lacking comparability across studies. Also, the susceptibility of bio-based insulations to moisture represents an additional aspect requiring further investigation, particularly regarding its influence on thermal conductivity, as highlighted by Palumbo et al. [7]. In addition, durability limitations and susceptibility to microbiological colonisation and degradation under high-moisture conditions have been reported for several bio-based insulations [4].

Within this context, tannin-based foams have emerged as a promising class of bio-insulations. Tannins are polyphenolic compounds extracted from renewable sources such as mimosa (*Acacia mearnsii*), quebracho (*Schinopsis* spp.), pine (*Pinus radiata*) and other tree barks [8–10]. Their high reactivity, particularly in the case of condensed tannins, enables the formation of rigid polymeric networks through reactions with aldehydes and furfuryl alcohol, producing lightweight foams with favourable thermal and fire-resistant properties [11]. Other studies have explored formaldehyde-free formulations and the incorporation of additives and catalysts to tailor foam morphology and mechanical performance [12].

Tannin-based foams offer several advantages over conventional synthetic foams, including intrinsic fire resistance, reduced toxicity and the potential for lower environmental

impacts due to their bio-based origin. Rodrigues et al. [13] demonstrated that sandwich panels with tannin foam cores exhibit promising thermal behaviour, suggesting their potential use in applications requiring enhanced fire protection. However, their performance remains highly dependent on formulation parameters, such as crosslinker type, catalyst concentration and the presence of reinforcing fibres. Understanding how these variables influence density, cell structure, thermal conductivity, moisture behaviour and mechanical properties is essential for optimising tannin foams for building applications.

Formaldehyde is often selected as a reference crosslinking agent because its reaction with tannins is well established and has been investigated in the development of tannin-based products. Condensed tannins contain highly reactive phenolic sites, particularly on the A-rings of the flavonoid units, which can react with formaldehyde through methylolation followed by condensation reactions, resulting in the formation of methylene bridges between tannin molecules and the development of a crosslinked three-dimensional network [14]. Nevertheless, the use of formaldehyde raises important health and safety concerns due to its high volatility and well-established carcinogenicity [15,16]. Glutaraldehyde can be investigated as an alternative to formaldehyde because of its bifunctional aldehyde structure, which provides two reactive aldehyde groups per molecule, in contrast with formaldehyde, which is monofunctional. Moreover, glutaraldehyde is less volatile than formaldehyde. The substitution of formaldehyde by glutaraldehyde may therefore provide an opportunity to reduce formaldehyde-related emissions while maintaining or improving the crosslinking efficiency and stability of the resulting composite. Li et al. [17] have studied glutaraldehyde as a substitute for formaldehyde in tannin/furanic foams. They reported that glutaraldehyde could completely replace formaldehyde under their optimised conditions, producing open-cell foams with good compressive resistance and thermal insulation. Yet, an earlier study by Lacoste et al. [18] reached a different conclusion: glutaraldehyde was found to be unsuitable for pine tannin/furanic foams because of its lower reactivity with pine tannins. Those studies demonstrate that the effectiveness of glutaraldehyde is strongly dependent on the tannin type and formulation. Moreover, the efficiencies of the two crosslinkers cannot be considered equivalent on a molar aldehyde basis, as glutaraldehyde differs from formaldehyde in molecular structure, reactivity and diffusion behaviour. Consequently, further investigation of the effect of formalin/glutaraldehyde substitution on the structure and performance of tannin-based foams remains relevant, particularly for the specific tannin source and formulation investigated in the present work.

It is expected that the present study contributes to this growing field by experimentally evaluating tannin-based foams produced with different crosslinkers and fibre addition. The objective is to assess how formulation affects key mechanical, hygrothermal and fire-related properties, and to determine the potential of these foams as sustainable insulation solutions aligned with circular-economy principles.

## 2. Materials and Methods

### *2.1. The Tannin-Based Foams*

Five formulations were produced and a minimum of three specimens of each, except formulation (v) for which only two were available, with average dimensions of 19.5 ($\pm$3.3) × 20.2 ($\pm$2.3) × 4.92 ($\pm$0.07) cm$^3$, were provided by the NTE Company Pty Ltd., Pietermaritzburg, KwaZulu-Natal, South Africa, using tannin extract produced from tree bark. The tannin extract was about 40% (by wt) in all the formulations. Two crosslinker agents—formalin (F) and glutaraldehyde (G)—were combined at different nominal proportions according to active aldehyde mass, namely: (i) 100% F; (ii) 50% F + 50% G; (iii) 25% F + 75% G; (iv) 100% G. The combination rates were defined by the company to assess the progressive replacement of formalin with glutaraldehyde (from 50% to 100%) while keeping

the number of formulations manageable, due to the limited amount of material produced. Moreover, as substitution of formaldehyde by glutaraldehyde may provide an opportunity to reduce formaldehyde-related emissions while maintaining or improving the crosslinking efficiency and stability of the resulting composite, it was a priority for the company to test higher percentages of glutaraldehyde (starting the substitution directly from 50% G).

Additionally, the formulation (v) at 50% F + 50% G was produced with the addition of fibres (Fr) from *Acacia mearnsii* (approx. 4% by wt of the other materials). The bark of *A. mearnsii* was selected for its high lignocellulosic fraction [19], with a hydroxyl-rich surface that may promote interactions with the phenolic tannin matrix, potentially contributing to the mechanical integrity and structural stability of the foam [20]. Furthermore, the lignin can promote the formation of more thermally stable carbonaceous residues during thermal degradation, which is of particular interest for the development of bio-based foams with improved fire performance [21]. Fibre incorporation was done at a single crosslinker ratio (50F-50G) and, therefore, the fibre-containing formulation was not intended to establish a general fibre effect independently of crosslinker composition. The 50F-50G formulation was selected for fibre incorporation because it represents an intermediate crosslinker composition, avoiding the exclusive use of either formalin or glutaraldehyde and, thereby, providing a mid-range formulation for assessing the additional contribution of fibre. Expansive agents, catalysers, reticulant agents and other products to favour tannin polymerisation added to the formulation are summarised in Table 1 and the production process, similar to the one detailed in a previous study [22], was the following: the water, furfuryl alcohol, crosslinker and PEG-400 were first mixed together in a 500 mL plastic beaker which was then fitted with an overhead stirrer. The tannin powder was then added portion-wise for over 5 min whilst stirring, and the resulting mixture then stirred for a further 15 min to ensure complete dissolution of the tannin. The Tween-80® was then added and stirred for 2–5 min, followed by the pentane, continuing stirring for 1 min. The beaker was then removed from the overhead stirrer, the p-TSA solution added in one portion and the resulting mixture stirred vigorously with a thick (10 mm) plastic stirring rod for 30 s, before being poured into a stainless-steel mould (210 × 250 × 40 $mm^3$). Once foaming had started, the mould was then placed into an oven at 105 °C for 15 min, before being allowed to cool for 20 min. The hardened foam was then demoulded and placed back in the oven for 10 min to finish curing, before being allowed to cool to RT overnight.

**Table 1.** Tannin foam composition by weight (wt%).

| Formulation | 100F | 50F-50G | 50F-50G (Fr) | 25F-75G | 100G |
|---|---|---|---|---|---|
| Tannin [%] | 41.5 | 41.3 | 39.7 | 41.4 | 41.4 |
| Water [%] | 8.3 | 5.8 | 5.6 | 5.2 | 3.6 |
| Furfuryl Alcohol [%] | 14.5 | 14.5 | 13.9 | 14.5 | 14.5 |
| Formalin 37% [%] | 9.8 | 5.1 | 4.9 | 3.1 | - |
| Glutaraldehyde 25% [%] | - | 7.5 | 7.2 | 9.9 | 14.6 |
| Aldehyde functionality [mol/100 g] | 0.121 | 0.100 | 0.096 | 0.088 | 0.073 |
| Active aldehyde mass [%] | 3.63 | 3.76 | 3.61 | 3.62 | 3.65 |
| PEG-400 [%] | 5.7 | 5.7 | 5.5 | 5.7 | 5.7 |
| Tween-80 [%] | 4.1 | 4.1 | 4.0 | 4.1 | 4.1 |
| Pentane [%] | 1.0 | 1.0 | 1.0 | 1.0 | 1.0 |
| p-TSA 65% [%] | 15.0 | 15.0 | 14.4 | 15.0 | 15.0 |
| Milled Bark Fibre [%] | - | - | 4.0 | - | - |

Note: The amount of added water changed to consider the more dilute glutaraldehyde solution; aldehyde functionality was calculated from the molar amount of aldehydes present in the formulation, considering the active contents of formalin (37 wt%) and glutaraldehyde solution (25 wt%), and the molecular weights of formaldehyde (30.03 g $mol^{-1}$) and glutaraldehyde (100.12 g $mol^{-1}$).

### 2.2. Commercial Insulation Products

Values for tannin foam (TF) from the literature are summarised in Table 2. For comparison, the main properties of some thermal insulation products accessible on the market are reported in Table 3, namely: (i) a polyurethane foam (PU) from Bostik Portugal [23]; (ii) an extruded polystyrene foam (XPS) from Danosa [24]; (iii) an expanded cork agglomerate panel also used on an ETICS [25]; and (iv) an expanded moulded polystyrene (EPS) used on an External Thermal Insulation Composite System (ETICS) [26].

**Table 2.** Values of apparent bulk density (BD), compressive strength (Fc) and thermal conductivity (λ) of tannin-based foams.

| Reference | BD [kg/m³] | Cs [MPa] | λ [W/(m·K)] |
|---|---|---|---|
| Celzard et al. [8] | 40–140 | 0.14–0.17 | n.a. |
| Lacoste et al. [9] | 35–190 | 0.06–0.14 | 0.033–0.037 |
| Čop et al. [10] | 99–102 | 0.09–0.16 | n.a. |
| Tondi et al. [11] | 56–115 | n.a. | 0.023–0.030 |
| Delgado-Sánchez et al. [12] | 22–69 | 0.02–0.18 | 0.037–0.045 |
| Borrero-López et al. [27] * | 30–200 | 0.05–1.75 | 0.032–0.070 |
| TF range | 22–200 | 0.02– 1.75 | 0.023–0.070 |

Notation: n.a.—not available; *—Literature review, values for TFF (tannin-furanic foams) were hereby considered.

**Table 3.** Technical characterisation of commercial insulating products as declared by producers.

| Ref | BD [kg/m³] | Cs [MPa] | λ [W/(m·K)] | μ [-] | FRC |
|---|---|---|---|---|---|
| PU | 20–30 | 0.10–0.30 | 0.030–0.035 | n.a. | B3 (DIN 4102-1) [28] |
| $XPS_{40}$ | 32 | ≥0.30 | 0.035 | ≥80 | E (EN 13501-01) [29] |
| $EPS_{40}$ | 20–25 | 0.10–0.15 | 0.034–0.036 | 30–70 | E (EN 13501-01) |
| ICB | ≤130 | ≥0.10 | ≤0.040 | n.a. | E (EN 13501-01) |

Notation: PU—Polyurethane; XPS—Extruded polystyrene; EPS—Expanded polystyrene; ICB—Expanded cork agglomerate; BD—Bulk density; Cs—Compressive strength; λ—Thermal conductivity; μ [-]—water vapour resistance factor; FRC—Fire resistance classification; B3—high flammability; E—high contribution to fire; n.a.—not available.

## 3. Test Methods

All properties were obtained as the average value out of three specimens (unless otherwise specified) obtained from different foam samples of the same formulation and, for comparison purposes, of the commercial insulations. For some tests, the specimens were cut into smaller samples, as defined for the respective test.

### 3.1. Density, Porosity and Mechanical Characterisation

For comparison, the tannin foams were tested together with expanded polystyrene (EPS) ISOVIT 150 [26] with 40 mm of thickness.

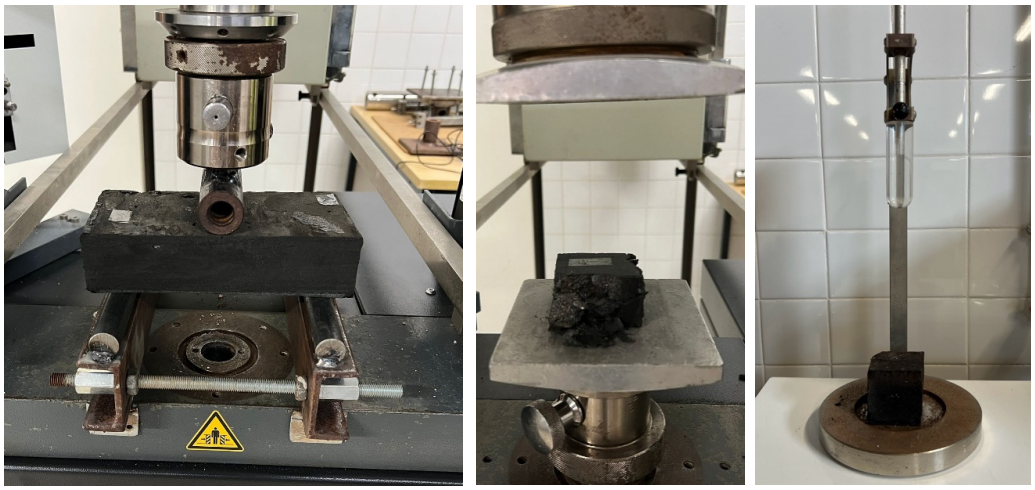
The bulk density (BD) was assessed on an average of three specimens (thickness 40–50 mm) for each composition. The specimens were conditioned at 19 ± 2 °C and 35 ± 3% RH (controlled laboratory conditions) and their volume geometrically determined with a digital caliper Macfer D304-20 (0.01 mm precision). Their mass was assessed using a balance with a precision of 0.001 g.

Scanning electron microscopy with energy dispersive X-ray spectrometry (SEM-EDS) observations were made at LNEC using a TESCAN MIRA 3 field emission microscope, TESCAN Group a.s., Brno, Czech Republic, combined with a BRUKER XFlash 6|30 EDS system, BRUKER Nano GmbH, Berlin, Germany. The samples were fractured (cutting

would compromise the observations) and coated by sputtering with gold. Observations were made in backscattered electron mode (BSE), with a chamber pressure of typically 20 Pa at an accelerating voltage of 15 kV.

The surface cohesion was evaluated following the variation proposed by Santos et al. [30] on the method described by Drdácký et al. [31]. An adhesive tape of 50 × 50 $mm^2$, previously weighed (0.001 g precision scale), was applied on three specimens of 200 × 190 $mm^2$ for each tannin-based foam and the EPS specimens. A neoprene fabric (for weight distribution) was placed on top of it, and a 2 kg weight was placed over the neoprene and left for 2 min.

The flexural strength (Figure 1a) was determined according to standard EN 12089 [32], with some modifications required by the dimensions of the available specimens. In fact, due to the original specimens' dimensions (maximum side of 200 mm), it was impossible to comply with the length requirements of method A (300 mm) or method B (250 mm). Consequently, the selected dimensions for the test were 200 × 80 $mm^2$ (with thickness between 40 and 50 mm). The test was run on three samples for each composition except for formulation (v), for which, due to sample shortage, only two specimens were available. A l Z050 universal testing machine, Zwick Roel, Ulm, Germany, was used with three bending points, a bearing distance of 150 mm, a loading cell of 50 kN and displacement speed of 10 ± 10% mm/min.



(**a**) (**b**) (**c**)

**Figure 1.** Determination of the mechanical properties: (**a**) flexural strength; (**b**) compressive strength; and (**c**) impact resistance.

The testing device for the assessment of the impact resistance (Figure 1c) of the foams was adapted from the plunger penetration test for the determination of consistence of fresh mortar [34] due to the reduced dimensions of the samples' surface (50 × 50 $mm^2$). The plunger (177.5 g), half-spherical pointed (diameter of 25.05 mm), was placed 150 mm from the upper surface of the specimen and dropped. The deformation of the samples' surface was measured with a digital caliper Macfer D304-20, ±0.01 mm of precision.

The compressive strength (Figure 1b) was determined on samples of 50 × 50 $mm^2$ (and original thickness) retrieved from the flexural test and conditioned at 23 ± 3 °C and 60 ± 2% RH. A Zwick Z050 device was used, with a pre-loading pressure of 250 ± 10 Pa followed by a displacement rate of 0.1 d/min, with d the original thickness (mm) of the specimen, as recommended by ISO 29469 [33]. The compression was applied until a deformation of the specimen equal to approx. 50% of its original thickness. The corresponding stress was used for the determination of the compressive strength (Figure 2).

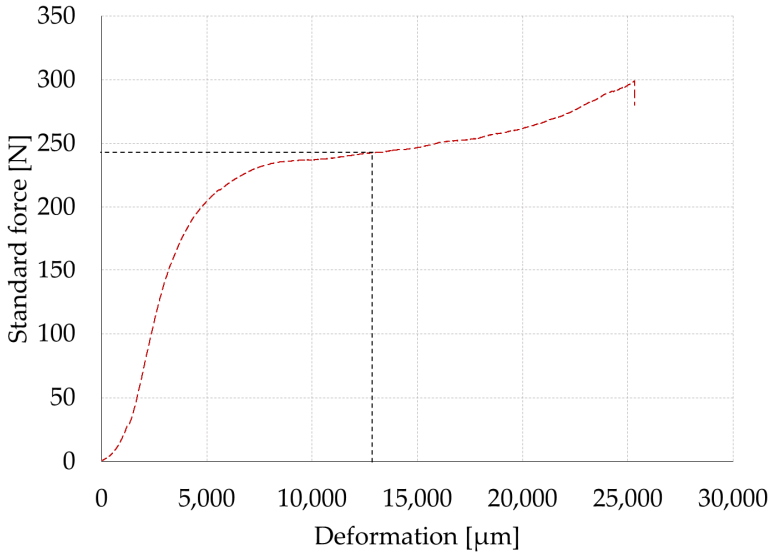



**Figure 2.** Representative stress–strain curve of the foams (dashed red line). In dashed black the 50% of total deformation (x-axis) and corresponding standard force (y-axis).

### *3.2. Thermal Conductivity*

The ISOMET 2114, Applied Precision s.r.o., Bratislava, Slovakia, equipment (Figure 3a) with an IPS1105 surface probe with 60 mm diameter and measurement range 0.04–0.3 W/(m·K) was used to measure thermal conductivity (λ) and volumetric heat capacity (cp) under three different hygrothermal conditions: (i) 20 °C and 20% RH, (ii) 23 °C and 50% RH and (iii) 23 °C and 80% RH. The thermal properties were assessed on three specimens for each tannin-based foam (200 × 190 mm$^2$) and three specimens of XPS CANDIWALL Board [35], EPS Isovit 150 [26] and ICB Isovit [25].



(**a**) (**b**) (**c**) (**d**)

**Figure 3.** Thermal conductivity test (**a**); samples prepared for capillary water absorption test (**b**); assembly for water vapour permeability test (**c**); water absorption for partial immersion test (**d**).

### *3.3. Water Vapour Permeability*

The water vapour permeability was assessed according to the wet cup method of the ISO 12572 [36] standard on samples of 110 × 110 mm$^2$, leaving an exposed surface area of 80 mm diameter on the top and bottom side of the system (Figure 3c). The cup was filled with water covered with cotton wool to avoid any contact between the specimens and the liquid water. Nevertheless, the air gap of minimum 15 mm height was ensured, to comply with the standard recommendations. The samples were sealed with aluminium tape and with mastic resin plus aluminium tape to the cup. The starting mass of the assembly (filled cup and sample, Figure 3c) was determined and the cup was placed in a climatic chamber at 23 °C and 50% RH. After two days of exposure, the assemblies were weighed every 24 h until steady state (mass variation below 5% for five successive weighing). The resistance

factor was calculated considering the water vapour permeability of air at the temperature of 23 °C from the Schirmer formula, equal to 1.952 $10^{-10}$ kg/(m·s·Pa).

### *3.4. Hygroscopicity*

The hygroscopic behaviour of the foams (only) was assessed according to the modified method suggested by Lima et al. [37] based on the German standard DIN 18947 [38]. Three specimens for each formulation were sealed with aluminium tape all along their thickness and base, leaving the top surface area of 200 × 190 $mm^2$ the only part in contact with air. After being stabilised in a climatic chamber at 23 °C and 50% RH and weighed to determine the starting mass, the RH of the chamber was increased to 80% for 24 h and back to 50% during the next 24 h. The 48 h test evaluated the moisture adsorption and desorption of the tannin-based foams returning the mass-variation curve (per unit surface area) by weighing at 1 h, 3 h, 6 h, 12 h and 24 h from the change in RH.

Moreover, the dimensional stability under the high RH level was determined according to EN 1604 [39], measuring the length variation, before (23 °C and 50% RH) and after (23 °C and 80% RH) the exposure, on the three dimensions.

### *3.5. Water Absorption*

The tests were run under laboratory conditions, 23 ± 3 °C and 60 ± 2% RH. Three specimens were tested for all the formulations (including EPS ISOVIT 150) except for formulation (v), for which only two replicates were available. The water absorption and thickness variation of specimens totally immersed in water for 2 h and 24 h were evaluated on samples of 50 × 50 $mm^2$ with a thickness of about 40–50 mm.

Additionally, bigger samples (90 × 110 $mm^2$) were totally immersed in water for 28 days, under the same conditions. Due to the tendency of the foams to float, a small weight was placed on top of each sample in both tests. Also, to ensure the surface water contact also on the bottom, a plastic net was used to place the samples.

The same test assembly was used to assess the water absorption by partial immersion (10 ± 1 mm soaked in water) according to ISO 29767 [40] for thermal insulation products. Samples of 50 × 50 $mm^2$ were used and weighed before and after being partially immersed for 24 h (Figure 3d), with a period of 10 min drying (before weighing) on a holder at 45° on horizontal surface.

To evaluate the capillary water absorption according to ISO 15148 [41], samples of 50 × 50 $mm^2$ (thickness between 40 and 50 mm) were sealed with wax (based on previous experimental campaigns made by the team for other bio-based building products) on their vertical faces (Figure 3b) and partially immersed in water (10 ± 1 mm height). The setup was the same as that used for the water partial immersion test with, in this case, a smaller water contact surface (net of sides). Mass variation was registered at 5 and 20 min, 1 h, 2 h, 4 h, 8 h, 24 h and 48 h from contact with water, placing the samples on a wet sponge just before weighing to remove extra water.

Next, the drying test was run following standard EN 16322 [42], specific for inorganic materials for conservation of cultural heritage. The samples were collected after the capillary water absorption test (not always saturated) and placed bottom-up. The first weighing occurred after 5 min, followed by five weighing within the first hour and one weighing per hour during the first 7 h. From there the samples were weighed every 24 h until reaching steady state (two consecutive daily mass variations below 0.1%). Following the requirements of the EN 16322 standard [42], the drying index (DI) [-] and the drying-phase rates $D_1$ [g/($m^2$·h)] and $D_2$ [g/($m^2$·$h^{0.5}$)] were calculated.

### *3.6. Contact with Flame*

The flame-reaction behaviour of the foams was evaluated through a simplified testing procedure, intended to highlight any differences between the foams and the commercial EPS. A simplified apparatus for the evaluation of ignitability [43] was built applying a 20 mm propane flame at a 45° angle at 10 mm to the specimen surface and about 40 mm above the bottom edge, sheltered with OSB panels on two sides (Figure 4a). The sample area exposed to flame was 110 × 90 $mm^2$, adapted to material availability from the 250 × 90 $mm^2$ recommended by the standard.



(**a**) (**b**)

**Figure 4.** Test assembly for reaction to fire test (**a**) and sample after the test (**b**).

Before testing, the samples were dried at 40 °C until constant mass, then hygrothermally conditioned in a laboratory environment and weighed to determine the test starting mass. The flame exposure lasted 30 s. The flaming droplets were quantified on filter papers (placed below the sample). The test (Figure 4b) allowed for the evaluation of critical reaction-to-fire parameters, including mass loss following flame application, the presence or absence of flaming droplets or particles, material ignitability, smoke release and the ability of the specimens to self-extinguish once the ignition source was removed. The test was also performed on EPS samples but not on XPS as this insulation is known for very rapid melting and smoke production.

The thermal stability analysis of the different foams was assessed by thermogravimetric analysis (TGA) performed using a Setaram Labsys EVO TGA (Caluire-et-Cuire, France) according to ASTM E1131 [44]. Approximately 5 mg of the sample was subjected to a temperature ramp up to 700 °C at a heating rate of 10 °C/min under both air and argon flow. The TGA curves under air and argon are included in the Supplementary Materials (S3). The residual mass at 550 °C, expressed as a percentage of the initial sample mass, was determined from the thermogravimetric curve obtained under an argon atmosphere to evaluate the char-forming behaviour of the foams. Separate measurements were performed under air to assess oxidative degradation and determine the residual inorganic ash fraction at 550 °C. The carbonaceous/char residue was estimated by subtracting the residual mass measured under air from that measured under argon, with both values expressed as percentages of the respective initial sample masses. The char residue obtained may help to assess whether the alteration of the crosslinker modifies the carbonaceous structure formed during decomposition [21].

### *3.7. Total and Leachable Trace Metals*

To evaluate how toxic the samples can be in terms of heavy metals, their total content was determined. Foams were incinerated in a muffle furnace (L3/11/C6, Nabertherm, Lilienthal, Germany), following ASTM E1755 [45]. The concentrations of lead (Pb), nickel (Ni), cadmium (Cd), chromium (Cr), zinc (Zn) and copper (Cu) were quantified in the nitric-acid-dissolved ash residues [46] by a high-resolution array inductively coupled plasma (ICP) optical emission spectrometer (Plasma Quant 9100 Elite, Analytik Jena, Jena, Germany). To evaluate the environmental toxicity of the materials, the amount of leached heavy metals was determined by ICP in the leachates obtained according to EN 12457 [47].

## 4. Results and Discussion

### *4.1. Density, Porosity and Mechanical Performance*

The bulk density (BD) of the foams ranged between 51 and 58 kg/m$^3$ (Figure 5), whereas the BD of the commercial EPS ISOVIT 150 is 20–25 kg/m$^3$ [26]. Among the tannin-based foams, those produced with 100% formalin and 100% glutaraldehyde had the lowest BD values (51 and 53 kg/m$^3$, respectively). The 25F-75G and 50F-50G (Fr) formulations followed, both with 57 kg/m$^3$. The 50F-50G formulation presented a slightly higher BD, reaching 58 kg/m$^3$. This behaviour suggests that density was influenced by the combined effects of crosslinker type and aldehyde functionality. Partial substitution with glutaraldehyde may have promoted earlier network formation, restricting foam expansion and resulting in higher apparent densities. However, increasing glutaraldehyde substitution was also accompanied by a progressive reduction in the total aldehyde functionality of the formulations (Table 1), due to the higher molecular weight of glutaraldehyde compared with formaldehyde. The lower concentration of reactive aldehyde groups in the 100G formulation may have reduced crosslinking efficiency, partially offsetting the effect of glutaraldehyde and resulting in lower density than that observed for the intermediate substitution levels.

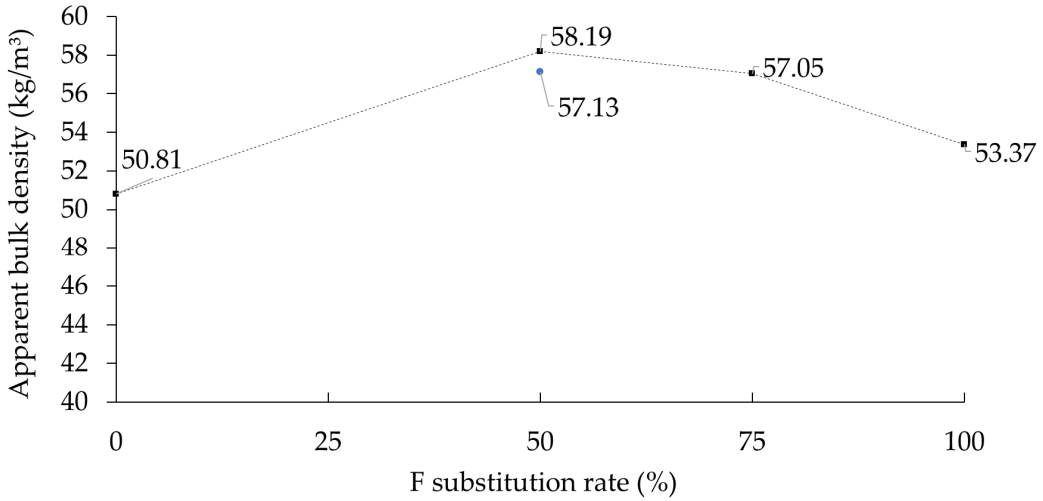



**Figure 5.** Average value of bulk density at increasing rates of F substitution with G (bottom); dot in blue corresponds to 50F-50G (Fr).

When the foams are produced using only one of the two crosslinker agents (F or G), the porous structure consists of small, rounded and relatively homogeneous pores (Figure 6A,D).

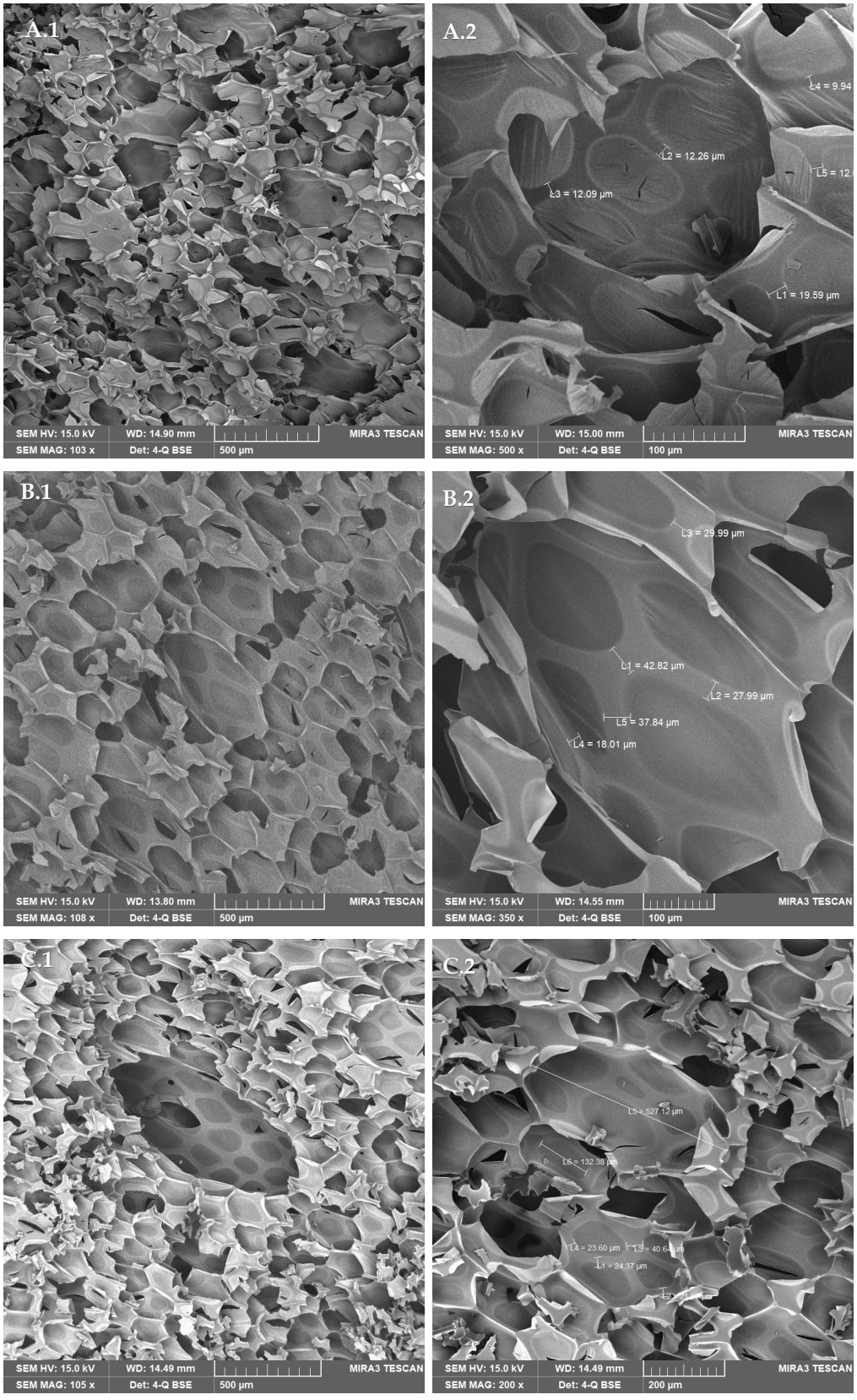



**Figure 6.** *Cont*.

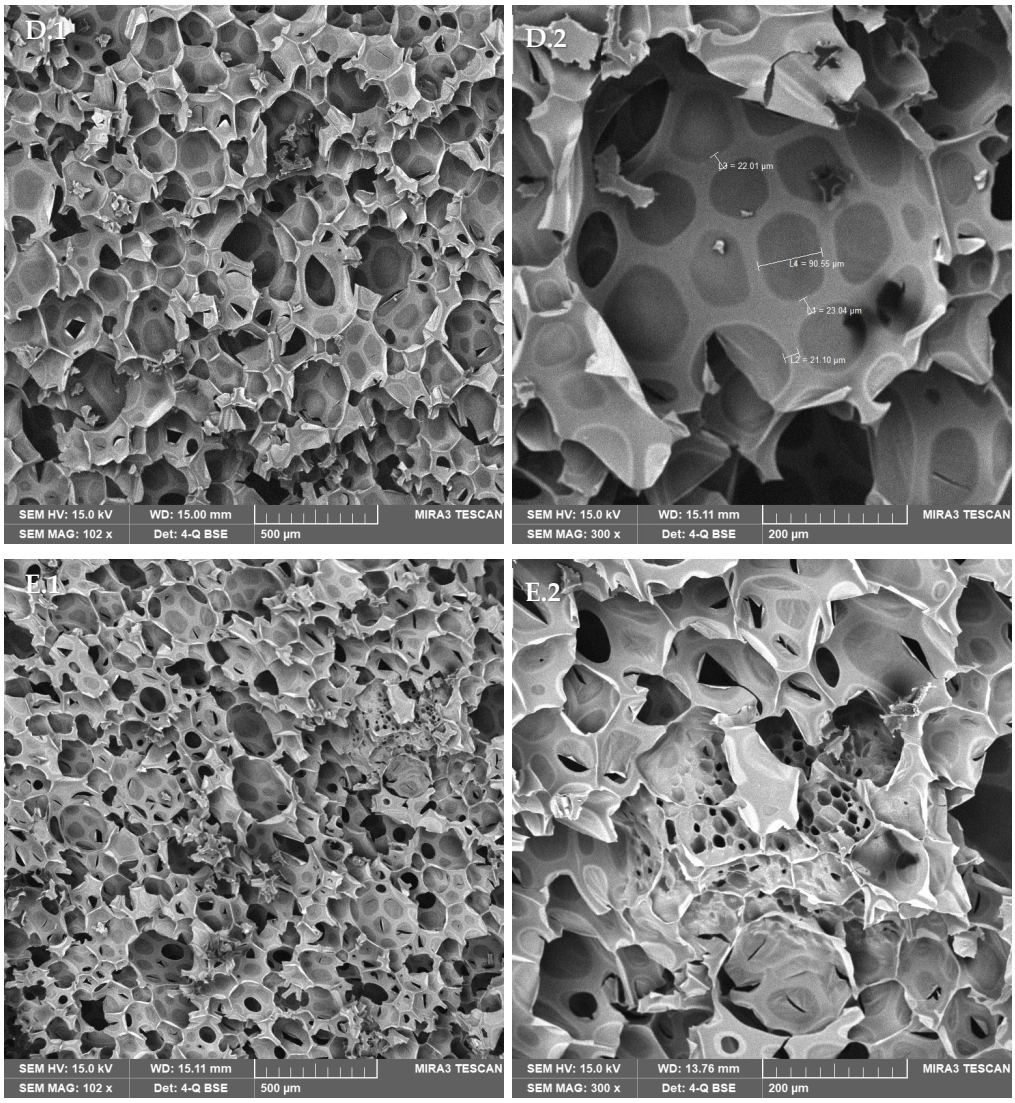


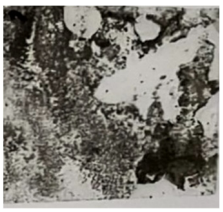

**Figure 6.** SEM images of the tannin foams: (**A**) 100F; (**B**) 50F-50G; (**C**) 25F-75G; (**D**) 100G; (**E**) 50F-50G (Fr).

When the two crosslinker agents are combined, additional pores with larger size and a more elongated morphology appear within the structure (Figure 6B,C,E). Moreover, in the formulation with the fibre addition, localised regions of denser and smaller porosity were observed (Supplementary Materials, S1 and S2). The appearance of larger, elongated pores in the hybrid F–G formulations is consistent with previous observations that crosslinker content and type strongly govern pore development in tannin-based systems. Čop et al. [10] showed that increasing the proportion of a di-aldehyde crosslinker (glyoxal) in tannin–furanic foams produced a more uniform cell size distribution, while lower crosslinker content favoured larger, less regular cells. This trend may explain the more heterogeneous porosity observed at intermediate F/G ratios in the present study. Similarly, Rodrigues et al. [13] attributed the irregular, larger-pore structure of formaldehyde-free tannin foams (compared with more homogeneous PU foams) to the high crosslinking rate of the furanic component, which promotes rapid, less controlled curing. These findings support the interpretation that the coexistence of two crosslinkers with different reactivity in the hybrid foams disrupts the regularity of cell nucleation and growth. A more quantitative analysis of pore size distribution was not considered reliable, as specimen fracture during sample preparation affected the integrity of most pores, hindering the accurate delineation

of pore boundaries. In addition, the presence of different focal planes within the images complicates the acquisition of representative measurements of the actual pore dimensions. Nevertheless, thicker cell walls were noticed in the images for the hybrid F–G formulations (that might be related to their higher density).

The material retained on the adhesive tape was used to assess the lack of surface cohesion of the foams (Table 4). All tannin foams and EPS showed similar material loss, with average value ranging 4–7% and small standard deviations (0.4–1.9%). However, despite the comparable quantities of material collected on the tape, the nature of the collected materials differed: for EPS it consisted mainly of surface dust accumulated on the specimens' surface. In contrast, the tannin-based foams released small particles when handled, indicating a different cohesive behaviour. Therefore, reduced surface cohesion is a documented limitation of tannin-based foams relative to synthetic insulants such as EPS. Azadeh et al. [48] identified surface friability, alongside excessive water uptake, as one of the most persistent drawbacks of tannin–furanic foams for insulation applications. This behaviour has been linked to the inherently brittle, highly crosslinked tannin–aldehyde network, which tends to release small particles from the cell walls upon handling rather than only surface dust. Strategies such as esterification of the tannin with fatty acids have been shown to markedly reduce or even eliminate friability [48]. This observation may suggest that the phenomenon is linked to the chemical and morphological nature of the polymer network, rather than being an unavoidable feature of bio-based foams.

**Table 4.** From top to bottom: referenced insulation foams average value (out of three measures) of material loss with (standard deviation); material loss observed on the adhesive tape.

| 100F | 50F-50G | 50F-50G (Fr) | 25F-75G | 100G | EPS |
|---|---|---|---|---|---|
| 4% (1.6) | 4% (0.9) | 6% (1.4) | 7% (1.9) | 4% (0.9) | 4% (0.4) |
|  |  |  |  |  |  |

Notation: 100F—100% formalin; 50F—50% formalin; 25F—25% formalin; 50G—50% glutaraldehyde; 75G—75% glutaraldehyde; 100G—100% glutaraldehyde; EPS—EPS Isovit 150.

The low-energy impact resistance was assessed following the adapted testing method to allow comparison among the highly deformable formulations. All the tannin foams, except 100G, showed similar deformation under impact (Figure 7). The addition of fibres had a positive effect, reducing the perpendicular deformation by approximately 20% and the imprint diameter by about 50%. The EPS and formulation 100G had no measurable deformation, consistent with their higher compressive strength. Although none of the foams would be suitable for External Thermal Insulation Composite System (ETICS) insulation boards (where high-energy impact resistance is required), their good thickness recovery suggests potential applicability in sandwich panel configurations. The absence of measurable deformation in the 100G formulation is consistent with reports that higher crosslinker content increases the rigidity of tannin-based networks. Chen et al. [49] showed that in condensed-tannin non-isocyanate polyurethane (NIPU) foams, compressive strength improved progressively with increasing glutaraldehyde content, attributing this to a higher degree of crosslinking of the polymer network. A similar stiffening effect of aldehyde crosslinking has been quantitatively demonstrated for pine tannin foams: Lacoste et al. [9] showed that formaldehyde-free pine tannin foams exhibited a nearly constant, density-

independent elastic modulus (~0.21–0.23 MPa), indicative of a weak, poorly consolidated network, whereas formaldehyde-crosslinked foams displayed a much steeper modulus–density relationship, confirming that aldehyde crosslinking is a primary driver of foam rigidity in tannin-based systems. However, this trend is not universal: Lacoste et al. [18] also found that glutaraldehyde performs poorly as a crosslinker for pine tannin specifically, owing to its lower reactivity compared with glyoxal. This is a reminder that the effect of glutaraldehyde is strongly tannin-source-dependent, and that *Acacia mearnsii* tannin (used in the present study) may behave differently from pine tannin in this respect. It should also be noted that Čop et al. [10], working with a different dialdehyde crosslinker (glyoxal), observed an inverse trend, with higher crosslinker content reducing compressive strength. That suggests that the relationship between crosslinker rate and stiffness is not necessarily monotonic and may depend on the specific aldehyde and formulation balance.

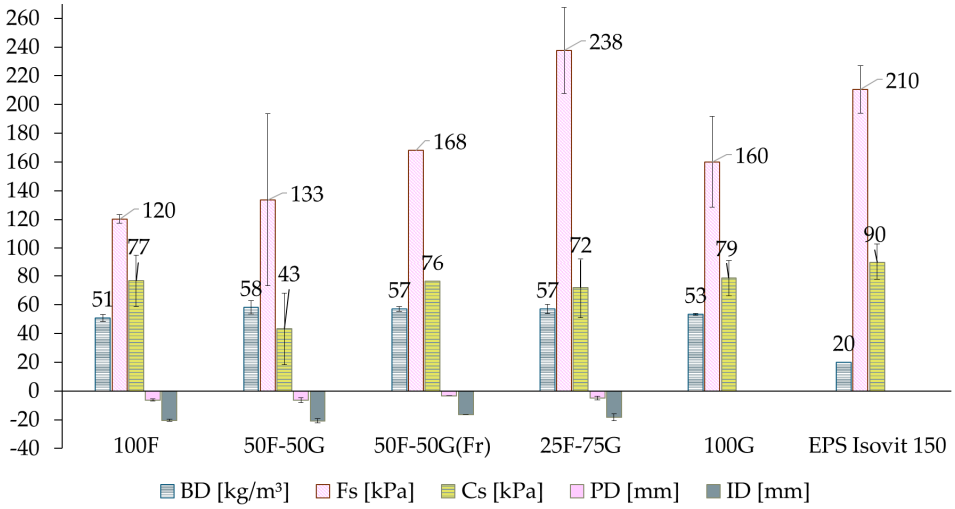



**Figure 7.** Bulk density (BD), flexural strength (Fs), compressive strength (Cs), perpendicular deformation (PD) and impact diameter of imprint (ID) by the impact test.

The flexural strength of the foams ranged from 120 to 238 kPa (Figure 7). Higher values were obtained for the formulations containing glutaraldehyde as the cross-linking agent, with the 25F-75G foam showing the best performance. The addition of fibres increased the flexural strength by approximately 25%. Only the tannin-based foam formulated with 75% glutaraldehyde exceeded the flexural strength of EPS Isovit 150.

The compressive strength was similar across all formulations, except for 50F-50G (Figure 7) that showed a lower value combined with higher standard deviation, ranging from 72 to 79 kPa, with values approximately 15% lower than EPS. According to Eckardt et al. [50], formaldehyde-free tannin foams with a density of about 50 kg/m$^3$ typically exhibit a mechanical resistance of about 30 kPa, a value more than doubled by the 100G formulation. The same researchers [50] highlighted that, beyond density, the most influential factor governing foams' compressive strength was the size and the distribution of the pores, observing that smaller and more homogeneous porosity led to higher compressive resistance. Nevertheless, the lower mechanical performance of formulation 50F-50G (43 kPa, approx. 40–46% lower than the other formulations) was associated with the highest standard deviation (±24.95 kPa), suggesting higher material heterogeneity. Results from flexural strength also pointed in the same direction. This might indicate that an equal proportion of the two crosslinkers leads to a more variable pore structure. However, this drawback was mitigated in the 50F-50G (Fr) formulation by incorporating *A. mearnsii* fibres, which restored the desired mechanical performance resulting in an approximately 75% increase in compressive strength (from 43 to 76 kPa). More importantly, the Cs variation between the two tested

50F-50G (Fr) specimens was about 12 kPa, more consistent with the SD observed for the other foams.

It is worth noting that the total aldehyde functionality decreased progressively from 0.121 to 0.073 mol per 100 g of formulation with increasing glutaraldehyde substitution. Nevertheless, neither compressive nor flexural performance followed this trend. While the 100G, with the lowest aldehyde functionality, achieved the highest compressive strength (within the small interval observed), the highest flexural strength was observed for the 25F-75G formulation. The compressive strength does not seem to vary markedly with crosslinker combination (excluding 50F-50G, due to its high SD), although aldehyde functionality decreased with increasing G substitution, and BD was lower for single-crosslinker formulations. On the other hand, the 25F-75G formulation showed an Fs definitely above the range observed for the other foams. These observations suggest that the mechanical behaviour of the foams cannot be explained solely by aldehyde functionality or bulk density.

During compression testing, the samples experienced thickness reductions of up to 53.5%, with partial recovery observed both immediately after unloading and after 24 h (Figure 8). Recovery reached up to 50% of the lost deformation in formulation 100F by the end of the test, and up to 75% in formulation 25F-75G after 24 h. The EPS did not follow the same recovery behaviour: it recovered more rapidly immediately after unloading, but its recovery slowed down thereafter, resulting in the highest residual deformation after 24 h, second only to formulation 100G. Rodrigues et al. [13] reported that tannin–furanic foams are predominantly open-celled, in contrast to the closed, well-interconnected cell structure of PU foams, a distinction that may similarly apply to differences in recovery behaviour between the more open-celled, glutaraldehyde-rich formulations and EPS, which is characterised by a closed-cell structure. Indeed, the comparatively rapid initial recovery followed by a slowdown observed for EPS is consistent with the general behaviour of closed-cell polymeric foams, in which entrapped gas provides fast elastic rebound immediately after unloading, while progressive strut/wall damage under sustained deformation can limit further recovery over time. The more open, irregular cell structure of the tannin-based foams likely introduced a slower viscoelastic response of the cell walls themselves, consistent with the progressive, delayed recovery observed over 24 h.

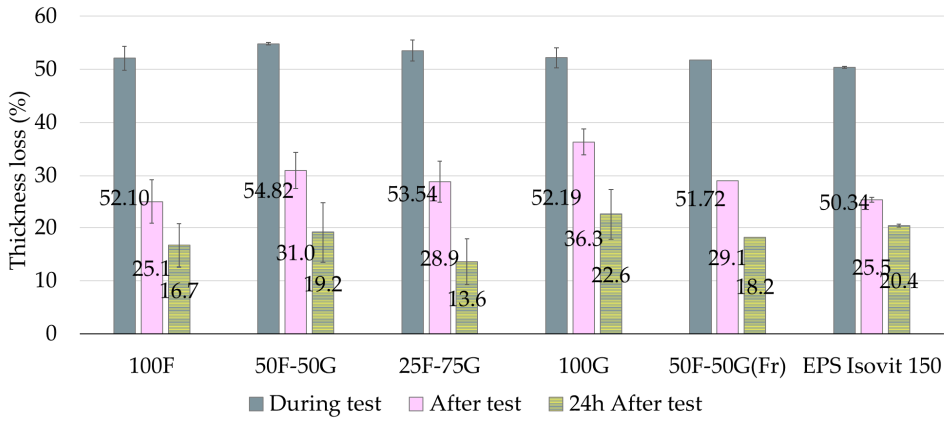



**Figure 8.** Thickness loss (%) due to the test, immediately after and 24 h after the compressive test.

The higher density observed for the intermediate glutaraldehyde substitution formulations is unlikely to result solely from the longer aliphatic chain of glutaraldehyde. Rather, it may be related to its bifunctional aldehyde structure and its ability to participate in intermolecular bridging reactions, which can promote the development of a more highly crosslinked network. In tannin-based systems, glutaraldehyde has been reported to exhibit high reactivity and to bridge tannin oligomers, resulting in earlier gelation and a higher

crosslinking level during the foaming process. This earlier network development can restrict foam expansion and stabilise the cell walls at an earlier stage, resulting in lower cell expansion, thicker cell walls and consequently higher apparent density [49]. The resulting increase in density and cell-wall thickness can, in turn, contribute to higher compressive strength, since the mechanical response of cellular materials is strongly dependent on relative density and cell-wall structure [51]. Chemically, the two aldehyde groups of glutaraldehyde can provide additional opportunities for intermolecular bridging, while its reaction kinetics with tannin can influence the rate at which the polymeric network develops. Physically, the timing of gelation relative to gas generation and solvent evaporation is expected to influence bubble nucleation, growth and stabilisation. A faster increase in viscosity and network formation can limit bubble growth and reduce cell coalescence, producing a denser and mechanically more robust cellular structure. This interpretation is consistent with previous studies showing that the reactivity of the crosslinking system strongly influences the morphology and mechanical properties of tannin-based foams [18,49].

The improvement in stiffness and strength observed after incorporation of fibre into the 50F-50G formulation can be attributed, at least in part, to interactions at the fibre–matrix interface. Lignocellulosic fibres contain abundant hydroxyl groups arising mainly from cellulose, hemicellulose and lignin, which can establish hydrogen-bonding and other secondary interactions with the hydroxyl and phenolic groups of the tannin matrix. Such interactions can improve interfacial adhesion and facilitate the transfer of applied stresses from the relatively rigid tannin matrix to the reinforcing fibre. Similar tannin–cellulose interactions have been reported to involve predominantly hydrogen bonding, van der Waals forces and CH–π interactions, with tannins becoming associated with the cellulose fibril surface [52]. In tannin-based foams specifically, incorporation of cellulosic fibres has been reported to reduce cell size and increase compressive strength, demonstrating the reinforcing effect of the fibre phase [53]. The fibre may, therefore, act not only as a physical reinforcement but also as a heterogeneous nucleation and cell-wall-stabilising phase during foaming, resulting in a more robust cellular structure. The hypothesis is consistent with SEM observation (Figure 6(E.1,E.2)) of scattered volumes of denser and smaller pores in 50F-50G (Fr). Nevertheless, since direct interfacial characterisation was not performed in the present study, these interactions should be regarded as the proposed mechanism rather than as experimentally demonstrated chemical bonding.

### *4.2. Thermal Conductivity*

All the tannin-based foams presented very similar thermal conductivity (λ), with very low standard deviation (Figure 9). Their moisture sensitivity was higher than that of conventional insulations (such as the XPS tested), showing an increase in thermal conductivity of about 20% when RH levels rose from 50% to 80%. Although this behaviour might be considered a drawback, it is worth noting that the increase of λ with RH is commonly observed in bio-based materials, due to their high hygroscopicity. For instance, Koh et al. [54] measured λ at different RH levels for bio-composites made of mycelium, hemp, grass and cork and found that highly hygroscopic composites, such as those based on mycelium, had a stronger increase in thermal conductivity with increasing RH. The same researchers [54] reported slope coefficients for the λ (RH) regression line of 0.0112, 0.0065 and 0.0094 for mycelium, hemp and grass-based, respectively, while cork-based showed no moisture sensitivity like the XPS tested in the present study. The slope coefficient of the λ (RH) fitting curve for the tannin-based foams falls within the range 0.0139 (100F) to 0.0177 (50F-50G). Palumbo et al. [7] observed comparable moisture-sensitive behaviour in bio-based composites, with slope values ranging from 0.015 for wood wool to 0.023 for hemp composites.

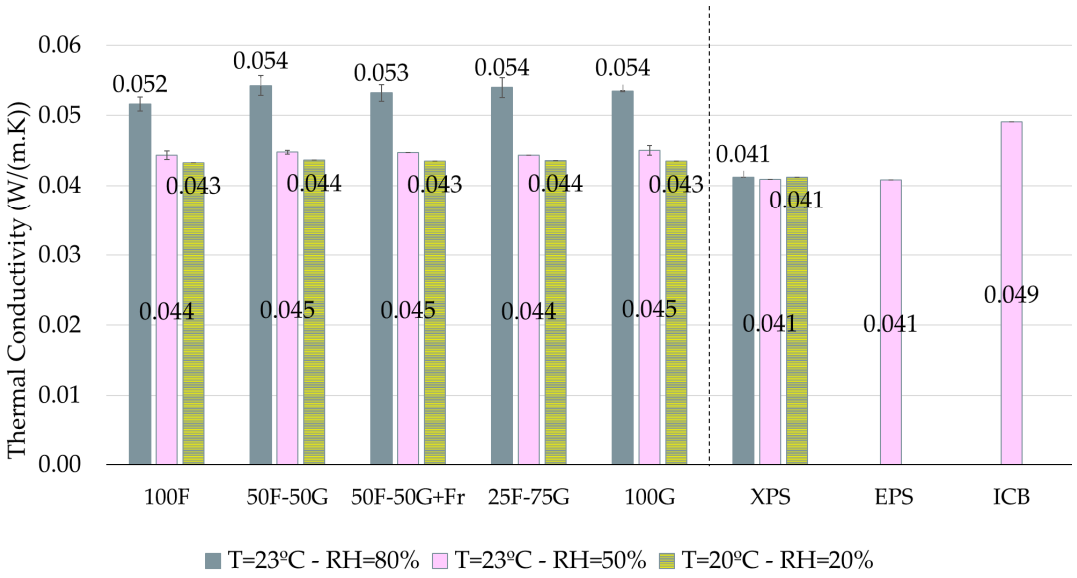



**Figure 9.** Thermal conductivity of the foams and XPS at three different hygrothermal conditions; thermal conductivity of EPS and ICB at intermediate RH condition. Dashed line separate tannin-based foams from conventional insulation materials.

Nevertheless, all foams were found suitable for thermal insulation purposes, with λ at 50% RH ranging between 0.044 and 0.045 W/(m·K), which lies in the mid-range of values reported in the literature for different studied insulations (Table 2). When compared with other bio-based insulation products (Figure 10) from Cosentino et al. [6] and Kumar et al. [55], values for tannin-based foams (in red) fall on the fitting curve, in the region (zoomed) corresponding to low-density/low-conductivity bio-based materials. Their thermal conductivity was only slightly higher (the measured differences of 0.002–0.003 W/(m·K) are not significant, as they fall within the uncertainty of the measurement system) than that of the EPS and XPS tested (0.041 W/(m·K)) and lower than that of ICB. Notably, the values found for all the tannin foams are close to the values declared for commercial insulation products (0.030–0.040 W/(m·K), Table 3).

Table 5 reports the volumetric heat capacity of the foams. The property rises steadily with increasing RH (like λ), reflecting the hygroscopic uptake of moisture within the porous structure consistently across all tannin-based formulations. The 25F-75G foam consistently shows the highest cp values at every condition, while 100F stays lowest among the foams, followed by 100G. The blended formulations (50F-50G and 50F-50G (Fr)) fall into an intermediate range, close to one another, indicating that fibre treatment has only a minor effect on thermal storage capacity. By contrast, XPS remains below all foam formulations and does not show any RH sensitivity, consistent with its high water vapour resistance factor (Table 3).

**Table 5.** Volumetric heat capacity (cp) under three different hygrothermal conditions: (i) 20 °C and 20% RH, (ii) 23 °C and 50% RH and (iii) 23 °C and 80% RH.

| **cp × $10^6$ [J/($m^3$ K)]** | **100F** | **50F-50G** | **50F-50G (Fr)** | **25F-75G** | **100G** | **XPS** |
|---|---|---|---|---|---|---|
| 20°C-20% RH | 0.120 ± 0.002 | 0.135 ± 0.013 | 0.136 ± 0.009 | 0.157 ± 0.009 | 0.126 ± 0.007 | 0.090 ± 0.002 |
| 23°C-50% RH | 0.133 ± 0.003 | 0.145 ± 0.013 | 0.151 ± 0.010 | 0.161 ± 0.023 | 0.137 ± 0.012 | 0.087 ± 0.001 |
| 23°C-80% RH | 0.178 ± 0.009 | 0.199 ± 0.024 | 0.204 ± 0.007 | 0.225 ± 0.026 | 0.204 ± 0.029 | 0.095 ± 0.000 |

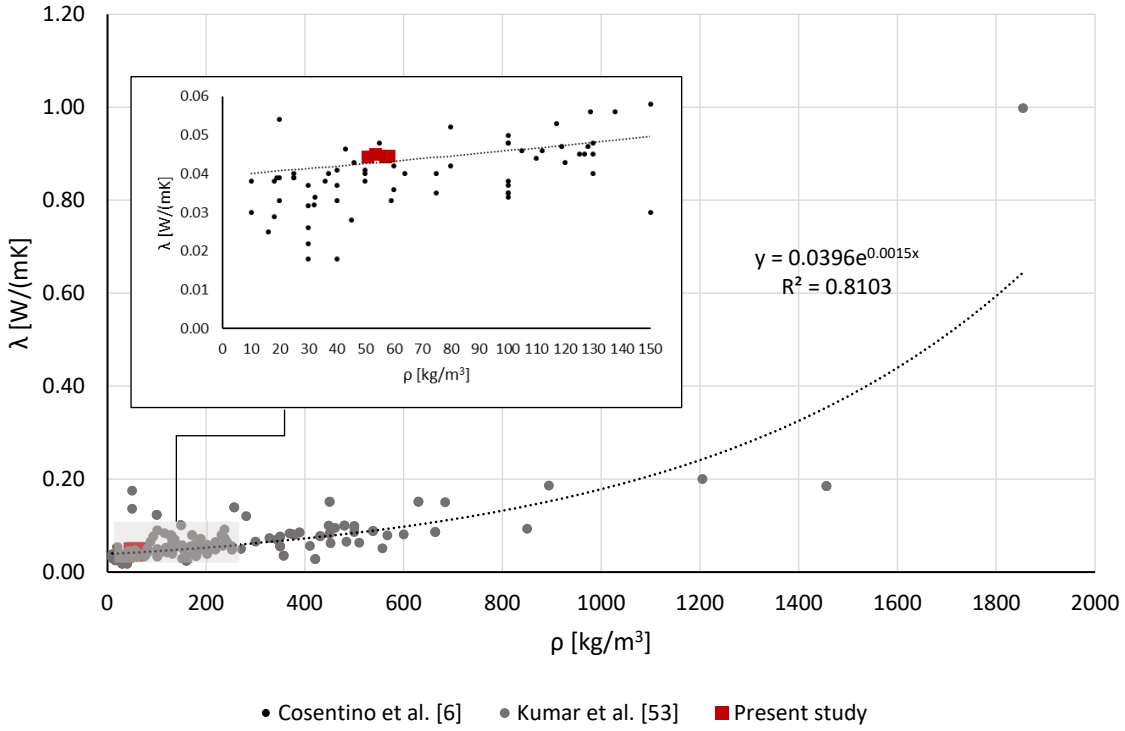



**Figure 10.** Thermal conductivity as a function of density for bio-based insulations. In red, tannin foams from the present study [6,53].

### *4.3. Water Vapour Permeability*

Water vapour permeability of tannin-based foams was found to be about nine times higher than for the commercial EPS tested under the same experimental conditions (Figure 11a). The resistance factor (μ) of EPS Isovit 150 was found to be approx. 16.5, significantly below the range 30–70 declared by the producer (Table 3). The tannin-based foams fell within the range of 1.60–1.90. A linear correlation with bulk density was found, with squared error of 0.97, except for the composition 50F-50G (Figure 11b, red square).

This result suggests that the combination of glutaraldehyde and formalin introduced a different porosity in the foam, as observed by SEM, leading to higher water vapour permeability. It is commonly known that natural-based construction systems, such as massive earthen walls or timber structures, as well as historic buildings, often require the addition of insulation systems (either during or after construction) to meet energy-performance standards [56]. Many of the insulating products available on the market present very high vapour resistance (30–70 for EPS and above 80 for XPS, as synthesised in Table 3) when compared with traditional building materials, for instance earth-based ones synthesised in Table 6. For this reason, bio-based insulations, such as the tannin foams here analysed, have interesting potential for this type of application. Also, according to Posani et al. [57], insulations with low capillary water absorption and high vapour permeability ensure the best compatibility with traditional masonry walls (granite, limestone and brick walls) under different climates (namely Porto, Lisbon and Bologna). Therefore, the low water vapour resistance suggests a potential interest of the bio-based tannin foams for this type of application.

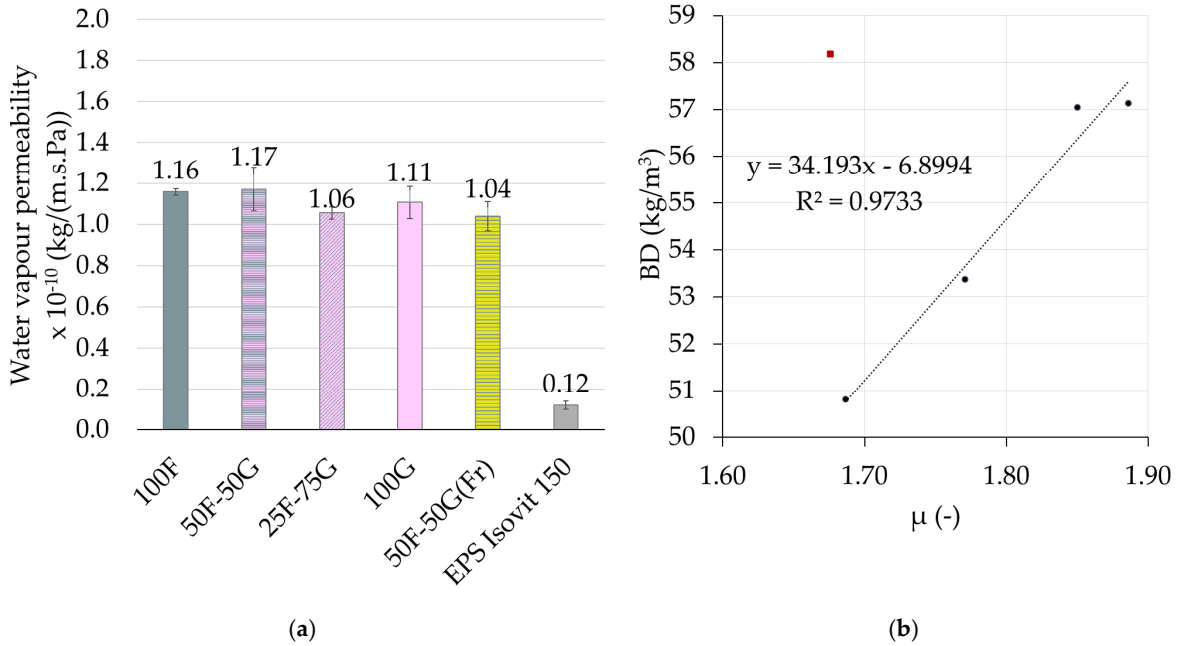



**Figure 11.** Water vapour permeability of the insulation foams (**a**); bulk density vs. water vapour resistance factor (μ); in red, out of the trendline, the formulation 50F-50G (**b**).

**Table 6.** Earth-based building materials: density and water vapour resistance factor from wet cup.

| Material | Bulk Density [kg/m$^3$] | μ-Value [-] | Study/Reference |
|---|---|---|---|
| Extruded brick | 1700–2100 | 3–7.1 | [58,59] |
| U-CEB | 1758–2046 | 5.5–11.1 | [60,61] |
| LS-CEB | 1728–1863 | 5.9–9.4 | |
| CS-CEB | 1683–1797 | 6.5–7.7 | [61] |
| RE | 1850–1850 | 7.8–9.1 | [62] |

Notation: CEB—compressed earth blocks; U—unstabilised (without addition of common binder); LS—lime stabilised; CS—cement stabilised; RE—rammed earth. μ-value [-]—water vapour resistance factor.

### *4.4. Hygroscopicity*

The highest moisture adsorption at the end of 24 h (Figure 12) was observed for 50F-50G (172 g/m$^2$), in agreement with the higher WPV (Section 4.3) and lower compressive strength.

Apart from 50F-50G and 100F, the other foams showed a similar behaviour, reaching approximately 160 g/m$^2$ of moisture uptake by the end of the adsorption phase. The lowest moisture content (143 g/m$^2$) was observed for the 100F formulation, which also showed the lowest residual moisture content at the end of the test (around 25 g/m$^2$), whereas the remaining formulations registered a residual moisture content of about 33–35 g/m$^2$. All the foams presented a residual moisture content by the end of the test, indicating that the desorption phase would likely have required a longer duration to be completed. Overall, all the foams showed hygroscopic behaviour comparable to that of earth-based plasters. Previous studies [30,37,63–65] identify earthen plasters as highly hygroscopic coatings, reporting moisture uptakes of approx. 80–140 g/m$^2$ after 24 h. These values depend on factors such as mortar composition, clay mineralogy, fibre incorporation and the use of additions. Therefore, the moisture uptake of 140–170 g/m$^2$ observed for the tannin-based foams aligns with the range typically observed for coatings with good hygroscopic capacity.

Moreover, it is worth noting that, for a moisture content of the foams in equilibrium with 80% RH, it was observed (Section 4.2) that the thermal conductivity remains relatively low (0.052–0.054 W/(m·K)), without jeopardising their insulation function.

After 48 h of exposure to 80% RH, all the foams presented a small volumetric expansion, in the range 6.75–7.60%. Nevertheless, because the standard deviations of the linear dimensional changes are relatively high (≈0.5%), a comparison between foams was excluded, as the propagated uncertainty would make the volumetric differences insufficiently reliable.

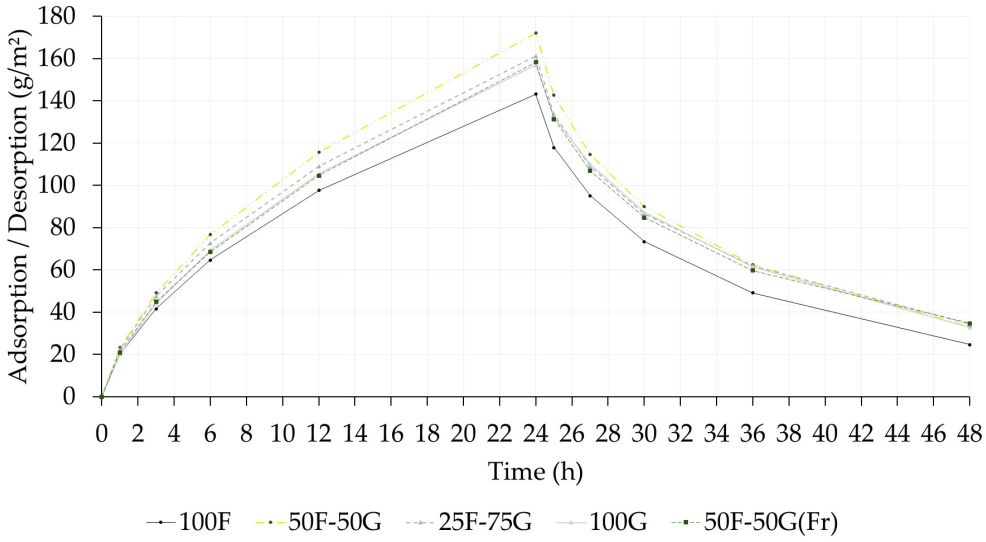



**Figure 12.** Moisture adsorption and desorption of the tannin foams.

### *4.5. Water Absorption*

The water uptake increases progressively with time for all foams (Figure 13). After 2 h and 24 h of total immersion, 100F absorbed the least among the foams, while 50F-50G (Fr) and 100G absorbed the most. The introduction of fibres increased the water absorption by approx. 10% at 24 h. By 28 days, however, 100F overtakes all others (1022.7%), while the other foams show a much smaller increase between 24 h and 28 d, with 25F-75G showing the lowest final absorption among the foams (833.3%). This crossover suggests that 100F has a slower initial uptake but a more sustained, long-term water absorption mechanism (progressive saturation of the internal porous network), whereas the G-containing foams and 100G approach saturation earlier and plateau. EPS remains far below all foams at every time point (as expected), but it shows a slight decrease from 24 h to 28 d, likely within measurement variability, suggesting that saturation is reached by 24 h.

Thickness increased for all the foams and the EPS (Figure 13) by 2 h total immersion, and kept increasing by 24 h, consistent with the progressive water uptake. Among the bio-based foams, 50F-50G shows the highest thickness variation at both immersion times, also with the largest standard deviation, indicating a less uniform swelling response across samples. The lower variation observed for 50F-50G (Fr) suggests the introduction of fibres helped stabilise dimensional behaviour despite showing little effect on water absorption itself. 100F, 25F-75G and 100G show intermediate variation. EPS, despite absorbing far less water overall, still shows non-negligible thickness variation although the SD was found quite high.

Results from 24 h partial immersion are reported in Table 7. After 24 h of partial immersion, 100F shows the highest average water absorption (4.370 kg/m$^2$) among all formulations, driven by strong sample-to-sample dispersion: two of the three specimens absorbed 5.104 and 5.483 kg/m$^2$, while the third absorbed only 2.524 kg/m$^2$, which explains

the high standard deviation (±1.610). All the other formulations show similar and more contained values (2.606–3.005 kg/m$^2$), suggesting that the G component reduces water uptake. The Fr addition introduces no substantial difference in the 50F-50G, indicating a limited effect on water resistance under this test condition. Finally, the EPS remains about two orders of magnitude below all other foams (0.049 kg/m$^2$), confirming its essentially hydrophobic behaviour.

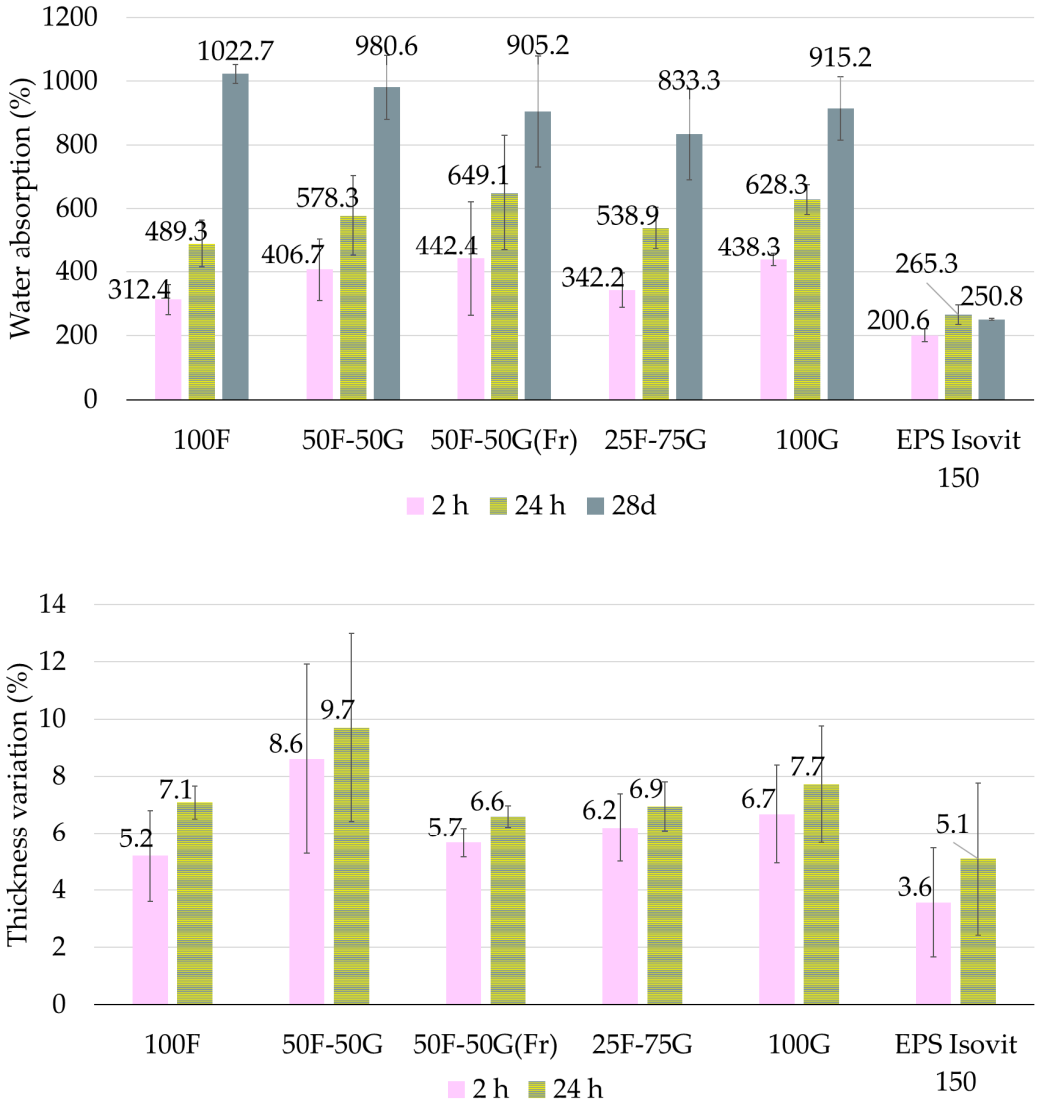



**Figure 13.** Water absorption of the foams (**up**) after 2 h, 24 h and 28 days of total immersion; and thickness variation (**bottom**) after 2 h and 24 h of total immersion.

**Table 7.** Water absorbed by partial immersion (24 h).

| | **100F** | **50F-50G** | **50F-50G (Fr)** | **25F-75G** | **100G** | **EPS Isovit 150** |
|---|---|---|---|---|---|---|
| Absorbed water [kg/m$^2$] | 4.370 | 3.005 | 2.857 | 2.606 | 2.619 | 0.049 |
| Standard deviation | 1.610 | 0.396 | 0.888 | 0.416 | 0.229 | 0.017 |

After 48 h of contact with water, capillary rise reached the upper face of the specimens and the test was ended. Nevertheless, as shown in Figure 14, none of the tannin foams reached saturation (horizontality of the absorption curve) by that time. However, there is evidence that the partial substitution of formalin (F) with glutaraldehyde (G) increased

the hydrophilicity of the foams. During the first 5 min, the 100G formulation absorbed the highest amount of water, although by the end of the test the highest absorption (3.72 kg/m$^2$) was recorded for the tannin foam with fibres addition. Indeed, the 50F-50G (Fr) formulation presented the first part of the curve (up to the first 4 h) more similar to the 25F-75G than the 50F-50G, indicating that the introduction of fibres affected the porosity of the foam (consistent with SEM), and a steeper slope in the final portion of the absorption curve, indicating that most probably water had begun to fill the smaller pores of the fibres and that this formulation would likely have reached a higher water content at saturation if the test had continued. As previously noted, the test was ended before saturation was achieved, but the drying curves likewise show a slower drying for this formulation in the first and second phases (Figures 14 and 15) compared with its fibre-free equivalent formulation (50F-50G), consistent with the presence of finer pores introduced by the fibres. As expected, the capillary water absorption of the EPS was almost negligible, reaching saturation after 23 h with 0.2 kg/m$^2$ of absorbed water.

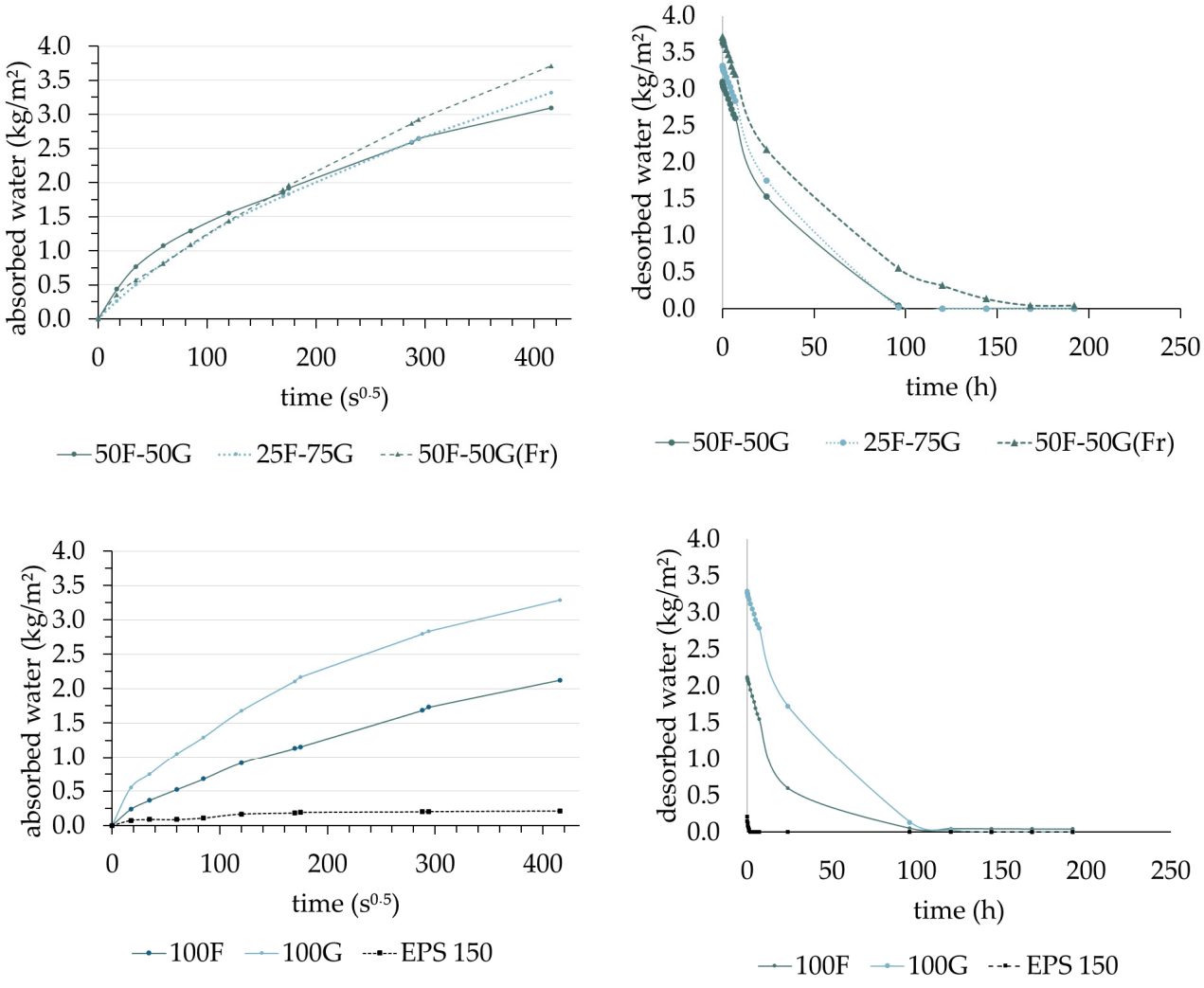



**Figure 14.** Capillary water absorption curves (**left**) and drying curves by time, allowing the determination of the first-phase drying rates (**right**).

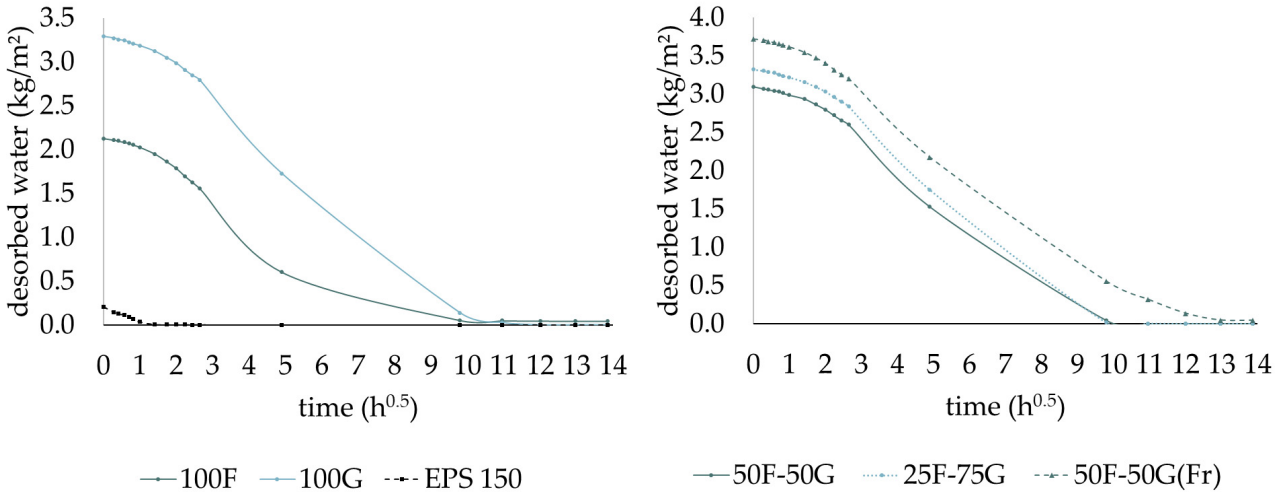



**Figure 15.** Drying curves by square root of time, allowing the determination of the second-phase drying rates.

The drying index after 120 h (DI) and the first ($D_1$) and second ($D_2$) drying rates were also calculated to improve the effectiveness of the comparison. The drying rates were determined over the intervals 0–7 h and 4–24 h, respectively, for all the foam samples, ensuring a coefficient of determination above 0.99. Due to its lower capillary water absorption and faster drying behaviour, the EPS required different calculation intervals (0–1 h and 0.5–3 h, respectively) with a slightly lower coefficient of determination (above 0.87). The results are presented in Table 8. The DI was found consistent with absorption behaviour, with the 100G formulation found to be the highest after 50F-50G (Fr) (the average value out of the two specimens is 0.191). The latter showed a high heterogeneity of results between the two tested specimens both for absorption and drying, possibly related to the distribution of the fibres within the specimens and during production. Indeed, the differences in drying reported in Table 8 (0.096 and 0.286) are consistent with the amount of absorbed water of the two samples at the end of 48 h (1.71 and 5.72 kg/m$^2$). The more hydrophobic behaviour of 100F was confirmed by its highest $D_1$ and the slowest drying in the first phase was observed for 25F-75G, although the latter was faster in releasing water vapour in the second phase. Almost all the formulations were completely dried after 120 h, except for 50F-50G(Fr), which presented the additional regions of smaller pores expected to dry slower.

**Table 8.** Drying Index (DI) at 120 h, first ($D_1$) and second ($D_2$) drying rates. Mean values ± standard deviation out of three specimens (except for 50F-50G (Fr) where the two obtained values are presented).

| | 100F | 50F-50G | 25F-75G | 100G | 50F-50G (Fr) | EPS |
|---|---|---|---|---|---|---|
| $DI_{120h}$ [-] | 0.099 ± 0.048 | 0.122 ± 0.036 | 0.131 ± 0.002 | 0.134 ± 0.057 | 0.096/0.286 | 0.010 ± 0.006 |
| $D_1$ [g/(m$^2$ h)] | 0.082 ± 0.001 | 0.071 ± 0.010 | 0.069 ± 0.006 | 0.071 ± 0.004 | 0.064/0.084 | 0.175 ± 0.026 |
| $D_2$ [g/(m$^2$ h$^{0.5}$)] | 0.408 ± 0.045 | 0.438 ± 0.052 | 0.442 ± 0.070 | 0.434 ± 0.087 | 0.343/0.504 | 0.085 ± 0.021 |

To assess the hygric compatibility with traditional masonry walls, in Figure 16, the $s_d$ value calculated for all the foams and EPS at a thickness of 50 mm is presented, together with their capillary water absorption after 24 h. Following the approach of Posani et al. [57], the figure also reports the accepted range for hygric compatibility defined in DIN 4108-3 [66] to prevent moisture accumulation in masonry walls. Although the German Standard specifically addresses rain-protective coatings, it is adopted as a comparative reference, despite not being originally formulated for tannin-based foams. All these foams present

low sd values, lying below the DIN [66] hyperbola ($A_w$ x $s_d$ = 0.2 (kg·m$^{-2}$·h$^{0.5}$)), but they show higher capillary water absorption than the limits typically prescribed for stucco and other coatings, with the exception of 100F. This behaviour indicates that the foams do not represent a protective barrier against liquid water, yet they would allow the substrate to dry efficiently. Consequently, the application of the tannin foams will require (based on this and the previous properties) a sandwich panel (where it could expand) or, if efficiently demoulded after expansion, a finishing layer or coating to ensure hygric compatibility and adequate protection against liquid water. In contrast, EPS acts as a stronger barrier to water vapour transport, while providing greater protection from wetting. Hence, if moisture transport occurs inside the masonry wall, its lower vapour permeability may result in slower drying of the wall, potentially promoting moisture-related degradation over time. If the aim is to protect historic masonry, the use of EPS would jeopardise that requirement.

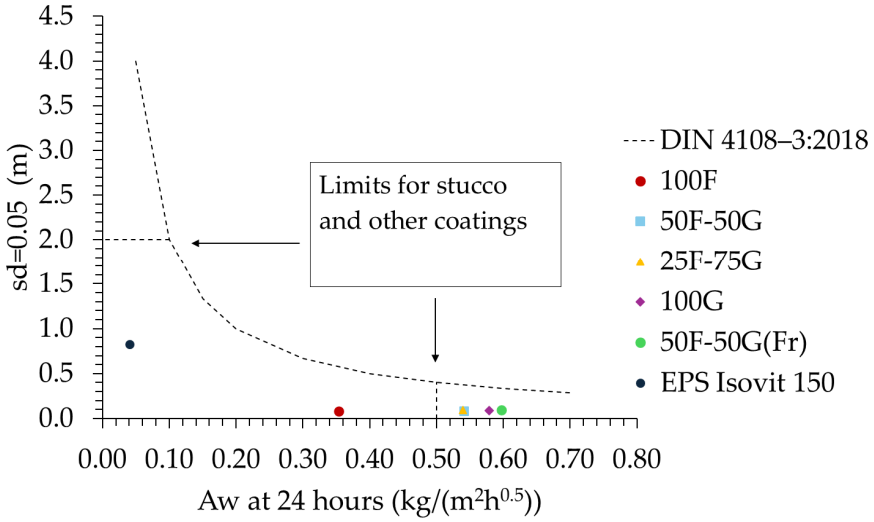



**Figure 16.** Thickness of the equivalent air layer ($s_d$) for a 0.05 m thickness and capillary water absorption coefficient ($A_w$) at 24 h. Limits set by the DIN 4108-3 [66].

### *4.6. Contact with Flame*

After contact of the foams with a flame, results (Figure 17) showed the absence of flaming droplets or particles. Also, no ignitability or smoke release was observed for any of the tested tannin-based insulations. No sustained flaming combustion was observed. After removal of the ignition source, only a small, localised smouldering glow remained, which self-extinguished within approximately 30 s without smoke production or flame development, except for the commercial EPS Isovit 150. The mass loss was quantified and is presented in Figure 17, together with images of the samples before and after the test. The whitish areas are only to allow marking the samples. These results are promising and consistent with the fire-safety advantages widely reported for tannin-based foams. Celzard et al. [67] found that tannin-based rigid foams exhibit outstandingly high fire retardance, with very difficult ignition and low heat release rates, explained by their ability to form a stable, low-conductivity char, and by their very low weight loss at ignition temperatures, since flame temperature is roughly proportional to weight loss. This mechanism is consistent with the behaviour observed: the absence of dripping and smoke, together with the rapid extinction of the residual glowing spot (unlike the EPS control), suggests a comparably low weight loss and stable char formation. Notably, Celzard et al. [67] also found that flame-retardant additives brought no significant improvement to tannin foams' already high fire retardance, suggesting that the extinction time of the residual glowing spot (approx.

30 s in the present study) likely reflects an intrinsic property of the tannin–furanic chemistry rather than a limitation to be corrected through formulation changes.

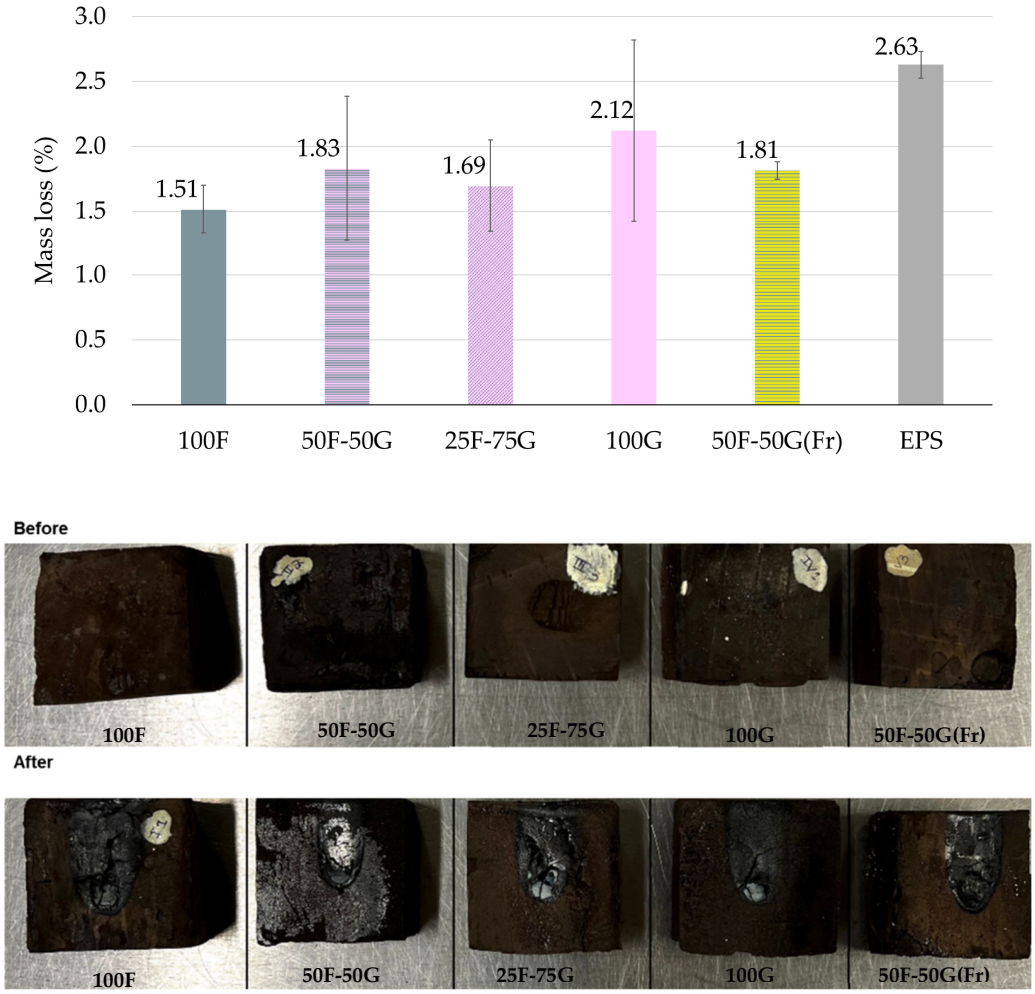



**Figure 17.** Quantified mass loss (%) after flame contact (**top**) and pictures of the tannin-based samples before and after flame contact (**bottom**).

Table 9 shows the char residual mass fraction of the foams.

**Table 9.** Char residual mass fraction of the foams, calculated as the percentage of the initial sample mass.

| Foam | 100F | 50F-50G | 50F-50G (Fr) | 25F-75G | 100G |
|---|---|---|---|---|---|
| (%) | 27.9 ± 0.1 | 27.9 ± 0.3 | 28.5 ± 0.4 | 28.5 ± 0.2 | 28.9 ± 0.2 |

The foams containing glutaraldehyde showed slightly lower decomposition than the formalin-only foam, indicating that replacing formalin with glutaraldehyde may result in a char with greater resistance to thermo-oxidative degradation. A similar effect was observed for the fibre-containing foam (50F-50G (Fr)), suggesting that the fibre incorporation also enhances the thermo-oxidative resistance of the char. Some authors report that the amount of residue after thermal degradation may be related to thermal stability and char protection behaviour, which can in turn be associated with fire resistance performance [21,68]. The higher residual mass observed for the glutaraldehyde-crosslinked foams may be related to differences in the crosslinked network: glutaraldehyde can act as a bifunctional crosslinking agent, promoting the formation of intermolecular bridges and potentially favouring the

development of thermally stable carbonaceous structures [49]. In addition, the glutaraldehyde molecule contains a three-carbon chain alongside its two aldehyde groups; during thermal degradation, the crosslinked organic network can undergo dehydration, condensation and aromatisation, resulting in a more thermally stable carbonaceous residue. For the 50F-50G formulation, fibre incorporation further increased the residual mass, which may result from both the mineral fraction of the fibre and its contribution to char formation, particularly relevant given the lignin-rich composition of *Acacia mearnsii*. Similar effects of fibre incorporation on char formation and thermal behaviour have been reported for tannin-based foams [21].

### *4.7. Total and Leachable Trace Metals*

Results of the analysis on the content of heavy metals and amount of leached heavy metals are presented in Tables 10 and 11.

**Table 10.** Heavy metals content in the foams.

| Formulation | 100F | 50F-50G | 50F-50G (Fr) | 25F-75G | 100G |
|---|---|---|---|---|---|
| Zn [mg/Kg] | 4.4 ± 0.5 | 5.5 ± 1.3 | 4.4 ± 0.4 | 6.2 ± 1.5 | 4.9 ± 0.9 |
| Cu [mg/Kg] | 4.1 ± 0.2 | 4.3 ± 0.4 | 2.9 ± 0.6 | 2.5 ± 0.1 | 2.8 ± 0.3 |
| Pb [mg/Kg] | 0.33 ± 0.02 | 0.33 ± 0.08 | 0.42 ± 0.08 | 0.45 ± 0.14 | 0.24 ± 0.09 |
| Ni [mg/Kg] | 0.65 ± 0.06 | 0.68 ± 0.16 | 0.81 ± 0.19 | 0.61 ± 0.08 | 0.68 ± 0.06 |
| Cr [mg/Kg] | 0.98 ± 0.05 | 1.02 ± 0.06 | 1.22 ± 0.27 | 0.98 ± 0.17 | 1.23 ± 0.30 |
| Cd [mg/Kg] | 0.25 ± 0.01 | 0.27 ± 0.03 | 0.25 ± 0.01 | 0.26 ± 0.01 | 0.24 ± 0.02 |

**Table 11.** Leached amount of heavy metals from the foams.

| Formulation | 100F | 50F-50G | 50F-50G (Fr) | 25F-75G | 100G |
|---|---|---|---|---|---|
| Zn [mg/L] | 0.041 ± 0.005 | 0.032 ± 0.005 | 0.038 ± 0.006 | 0.042 ± 0.005 | 0.038 ± 0.003 |
| Cu [mg/L] | nd | nd | nd | nd | nd |
| Pb [mg/L] | nd | nd | nd | nd | nd |
| Ni [mg/L] | nd | nd | nd | nd | nd |
| Cr [mg/L] | nd | nd | nd | nd | nd |
| Cd [mg/L] | nd | nd | nd | nd | nd |

Notation: nd—under the detection limit.

In terms of heavy-metal content (Table 10), the results show that the formulations containing glutaraldehyde do not differ from the 100F control. For copper (Cu), a small reduction is observed when formalin is replaced by glutaraldehyde. These findings indicate that the substitution of F with G did not increase the total heavy-metal content of the foams and that no additional heavy-metal-related environmental hazard is associated with the use of glutaraldehyde. This is consistent with the fact that heavy metals in tannin-based foams originate from additives (e.g., flame retardants, fillers, stabilisers) rather than from the aldehyde crosslinker itself [69]. Nevertheless, when developing new building materials and products, such as these tannin-based foams, the determination of heavy-metal content should always be included since the tannin source may be contaminated with heavy metals and could therefore influence the final quality and toxicity.

Regarding the amount of leached heavy metals from the different formulations (Table 11), which is relevant for evaluating potential environmental toxicity at the end of the life cycle of the product, Cu, Pb, Ni, Cr and Cd were not detected in the leachates of either the formalin-based foam or the glutaraldehyde-based formulations. This further supports the suitability of substituting F with G in terms of sustainability.

Only zinc (Zn) was detected in the leached samples, but no differences were observed among formulations containing G and the 100F foam. This metal is characterised by high mobility within materials compared to other micronutrients, which directly affects its transport and behaviour in industrial applications. This behaviour is typically associated with Zn being often present in additive-related or weakly bound phases that can migrate or leach under environmental exposure conditions [70].

## 5. Conclusions

This study asked whether glutaraldehyde could replace formalin in *Acacia mearnsii* tannin–furanic foams without compromising their function as thermal insulation. The answer is conditionally positive: replacing one crosslinker with the other did not act linearly, so the outcome depends on how the substitution is made. Foams with a single crosslinker (100F and 100G) developed fine, homogeneous cells, whereas combining the two aldehydes produced less regular porosity and higher densities. Neither density nor aldehyde functionality alone explained the mechanical response, which is more consistent with the interplay between crosslinker reactivity, gelation timing and cell stabilisation during foaming, an interpretation that still requires direct verification. Full substitution (100G) matched or exceeded the strength of the formalin foam, and 75% substitution gave the highest flexural strength, whereas the 50–50 mixture exhibited the highest dispersion in compressive and flexural test results, suggesting greater variability and possible heterogeneity during production. The substitution ratio should therefore be optimised rather than assumed to give intermediate properties.

Fibre addition behaved as a corrective measure rather than a general reinforcement; its influence on the porous structure must be further investigated, although some additional SEM and EDS observations are presented in Supplementary Materials. In the 50–50 matrix, the fibre addition did not jeopardise compressive or flexural strength, increased low-energy impact resistance and reduced swelling in water. On the other hand, it introduced a smaller porosity that increased capillary uptake and slowed down the drying (with 50F-50G(Fr) the only formulation not fully dried after 120 h). Since fibres were tested at a single content, in a single matrix and with only two specimens, their effect, namely on pore size distribution, should be further investigated.

Across the hygrothermal tests, the foams behaved as open, hygroscopic and vapour-permeable materials. Their thermal conductivity at 50% RH was only slightly above that of the EPS and XPS tested but rose by about 20% at 80% RH, their vapour resistance was roughly nine times lower than that of EPS and their moisture uptake was comparable to that of earth-based plasters. These advantages come with trade-offs: high capillary water uptake with no barrier against liquid water, a friable surface and a compressive strength about 15% below that of EPS. The foams are therefore better suited to protected configurations, such as sandwich panels or coated layers, and to permeable masonry where drying capacity matters, than to exposed boards or ETICS.

In the simplified flame test, none of the foams produced flaming droplets or released smoke. A brief and localised smouldering phenomenon was observed after removal of the ignition source; however, it did not propagate and self-extinguished within approximately 30 s. Moreover, the char residues were similar across formulations (about 28–29%), with at most a marginal increase with glutaraldehyde and fibre. This suggests that fire behaviour is governed mainly by the tannin–furanic matrix rather than by the crosslinker. The total and leachable heavy-metal contents were also unaffected by the substitution, with only zinc detected in the leachates.

The main motivation for replacing formalin, the lower volatility of glutaraldehyde, was not assessed, and aldehyde emissions remain the key open point. The findings are also

limited to one tannin source, one fibre type and content, a small number of specimens and some simplified macroscopic tests; the study establishes feasibility and trends rather than an optimised formulation. Future work should quantify pore structure and gelation kinetics, measure formaldehyde and other volatile emissions, vary fibre content independently of the crosslinker ratio, reduce water uptake and friability through hydrophobic or surface treatments and assess durability, acoustic performance and life-cycle impacts.

Overall, with respect to the properties assessed, glutaraldehyde is a viable partial or full substitute for formalin, provided the formulation is tuned to the intended application, which keeps tannin-based foams a promising bio-based option for protected, permeable (to water vapour) building solutions.

**Supplementary Materials:** The following supporting information can be downloaded at: https://www.mdpi.com/article/10.3390/su182110730/s1, Figure S1 (A–E): SEM images of the tannin foams; Figure S2: EDS analysis of 50F-50G (Fr), Figure S3: Thermogravimetric analysis (TGA) curves of the foams in air (A) and under argon (B).

**Author Contributions:** Conceptualisation, A.R. and P.F.; methodology, P.F. and A.L.F.; validation, A.R., P.F. and A.L.F.; formal analysis, A.R., P.F. and A.L.F.; investigation, A.R., P.F., A.S.S. and A.L.F.; resources, P.F., A.S.S. and A.L.F.; data curation, A.R.; writing—original draft preparation, A.R.; writing—review and editing, P.F. and A.L.F.; project administration, P.F.; funding acquisition, P.F. and A.L.F. All authors have read and agreed to the published version of the manuscript.

**Funding:** The Portuguese Agency for Innovation (ANI) funding COM-PETE2030-FEDER-00365700, operation 12706. This research was funded by EUROGIA 2030 project Morewood, ID number EU2030-19-2, and in part by the Fundação para a Ciência e a Tecnologia, I.P. (FCT, https://ror.org/00snfqn58, accessed on 10 August 2026, under Grant UID/6438/2025 (https://doi.org/10.54499/UID/06438/2025) of the research unit CERIS. This work was also supported by Fundação para a Ciência e Tecnologia, FCT/MECI through the MEtRICs research unit (UID/04077/2025, https://doi.org/10.54499/UID/04077/2025, Mechanical Engineering and Resource Sustainability Center).

**Institutional Review Board Statement:** Not applicable.

**Informed Consent Statement:** Not applicable.

**Data Availability Statement:** The raw data supporting the conclusions of this article will be made available by the authors on request.

**Acknowledgments:** The authors thank the NTE Company Pty Ltd. and Dino Clarke for providing the tannin-based insulation specimens. Acknowledgement is given to Diogo Jacinto for the experimental work conducted as part of his thesis and to Vitor Silva and Tânia Santos for the technical support provided during the experimental campaign. During the preparation of this manuscript/study, the author(s) used Microsoft 365 Copilot and Claude Sonnet 5.5 for language-improvement purposes. The authors have reviewed and edited the output and take full responsibility for the content of this publication.

**Conflicts of Interest:** The authors declare no conflicts of interest.

## References

1. European Environment Agency (EEA). *Buildings and Construction*; European Environment Agency (EEA): Copenhagen, Denmark, 2026. Available online: https://www.eea.europa.eu/en/topics/in-depth/buildings-and-construction (accessed on 16 March 2026).
2. Lu, Z.; Ambaye, T.G.; Mao, R.; Hauschild, M.; Ottosen, L.M.; Montalbano, G.; Zerbino, P.; Aloini, D.; Lima, A.T. Resource efficiency for closed-loop circularity of building insulation materials in Europe. *Sustain. Prod. Consum.* **2026**, *65*, 1–15. [CrossRef]
3. Mort, R.; Vorst, K.; Curtzwiler, G.; Jiang, S. Biobased foams for thermal insulation: Material selection, processing, modelling, and performance. *RSC Adv.* **2021**, *11*, 4375–4394. [CrossRef] [PubMed]

4. Raja, P.; Murugan, V.; Ravichandran, S.; Behera, L.; Mensah, R.A.; Mani, S.; Kasi, A.; Balasubramanian, K.B.N.; Sas, G.; Vahabi, H.; et al. A review of sustainable bio-based insulation materials for energy-efficient buildings. *Macromol. Mater. Eng.* **2023**, *308*, 2300086. [CrossRef]
5. Lu, Z.; Hauschild, M.; Ottosen, L.M.; Ambaye, T.G.; Zerbino, P.; Aloini, D.; Lima, A.T. Climate mitigation potential of biobased insulation materials: A comprehensive review and categorization. *J. Clean. Prod.* **2024**, *470*, 143356. [CrossRef]
6. Cosentino, L.; Fernandes, J.; Mateus, R. A review of natural bio-based insulation materials. *Energies* **2023**, *16*, 4676. [CrossRef]
7. Palumbo, M.; Lacasta, A.M.; Holcroft, N.; Shea, A.; Walker, P. Determination of hygrothermal parameters of experimental and commercial bio-based insulation materials. *Constr. Build. Mater.* **2016**, *124*, 269–275. [CrossRef]
8. Celzard, A.; Zhao, W.; Pizzi, A.; Fierro, V. Mechanical properties of tannin-based rigid foams undergoing compression. *Mater. Sci. Eng. A* **2010**, *527*, 4438–4446. [CrossRef]
9. Lacoste, C.; Basso, M.C.; Pizzi, A.; Laborie, M.-P.; Celzard, A.; Fierro, V. Pine tannin-based rigid foams: Mechanical and thermal properties. *Ind. Crops Prod.* **2013**, *43*, 245–250. [CrossRef]
10. Čop, M.; Lacoste, C.; Conradi, M.; Laborie, M.-P.; Pizzi, A.; Sernek, M. The effect of the composition of spruce and pine tannin-based foams on their physical, morphological and compression properties. *Ind. Crops Prod.* **2015**, *74*, 158–164. [CrossRef]
11. Tondi, G.; Pizzi, A.; Olives, R. Natural tannin-based rigid foams as insulation for doors and wall panels. *Maderas Cienc. Tecnol.* **2008**, *10*, 219–227. [CrossRef]
12. Delgado-Sánchez, C.; Santiago-Medina, F.; Fierro, V.; Pizzi, A.; Celzard, A. Optimisation of "green" tannin-furanic foams for thermal insulation by experimental design. *Mater. Des.* **2018**, *139*, 7–15. [CrossRef]
13. Rodrigues, M.B.B.; Côrrea, R.; De Cademartori, P.H.G.; Ribeiro, A.C.R.; Coldebella, R.; Delucis, R.A.; Lunkes, N.; Missio, A.L. Bio-based tannin foams: Comparing their physical and thermal response to polyurethane foams in lightweight sandwich panels. *Compounds* **2024**, *4*, 1–16. [CrossRef]
14. Braghiroli, F.L.; Amaral-Labat, G.; Boss, A.F.N.; Lacoste, C.; Pizzi, A. Tannin gels and their carbon derivatives: A review. *Biomolecules* **2019**, *9*, 587. [CrossRef] [PubMed]
15. IARC. Formaldehyde, 2-Butoxyethanol and 1-tert-Butoxypropan-2-ol. In *IARC Monographs on the Evaluation of Carcinogenic Risks to Humans*; International Agency for Research on Cancer: Lyon, France, 2006; Volume 88.
16. Environmental Protection Agency (EPA). *Facts About Formaldehyde*; U.S. Environmental Protection Agency (EPA): Washington, DC, USA, 1859. Available online: https://www.epa.gov/formaldehyde (accessed on 10 August 2026).
17. Li, X.; Pizzi, A.; Zhou, X.; Fierro, V.; Celzard, A. Formaldehyde-free prorobinetinidin/profisetinidin tannin/furanic foams based on alternative aldehydes: Glyoxal and glutaraldehyde. *J. Renew. Mater.* **2015**, *3*, 142–150. [CrossRef]
18. Lacoste, C.; Basso, M.C.; Pizzi, A.; Laborie, M.-P.; Garcia, D.; Fierro, V. Bioresourced pine tannin/furanic foams with glyoxal and glutaraldehyde. *Ind. Crops Prod.* **2013**, *45*, 401–405. [CrossRef]
19. Rodrigues, L.; Pedroso, P.d.C.; de Freitas, J.H.C.; de Oliveira, A.L.; Missio, A.L. Obtaining of a rich-cellulose material from black wattle (Acacia mearnsii De Wild.) bark residues. *Environ. Sci. Pollut. Res.* **2023**, *30*, 113055–113067. [CrossRef] [PubMed]
20. Zhou, X.; Li, B.; Xu, Y.; Essawy, H.; Wu, Z.; Du, G. Tannin-furanic resin foam reinforced with cellulose nanofibers (CNF). *Ind. Crops Prod.* **2019**, *134*, 107–112. [CrossRef]
21. Lazko, J.; Mariage, J.; Joyet, C.; Layachi, A.; Satha, H.; Dubois, P.; Laoutid, F. Toward safer and greener insulation: Formaldehyde-free, flame-retardant, and bio-based phenolic foams from tannin and modified-lignin combination. *Materials* **2026**, *19*, 334. [CrossRef] [PubMed]
22. Clarke, D.; Faria, P.; van Kralingen, L.; Arslan, G.B. Eco-Efficient Tannin-Based Insulation Foams. In *Proceedings of the 2nd International Conference on Net-Zero Built Environment (NTZR 2025) Lecture Notes in Civil Engineering*; Beushausen, H., Kioumarsi, M., Shafei, B., Eds.; Springer: Cham, Switzerland, 2026; Volume 873. [CrossRef]
23. Bostik Portugal, S.A. P300 Foam'n'Fill B3—Polyurethane Foam. In *Technical Sheet (in Portuguese)*; Bostik Portugal, S.A.: Lisbon, Portugal, 2023. Available online: https://www.bostik.com/portugal/pt/catalog/product/construction/emea/portugal/product-bostik-p300-espuma-poliuretano-manual/ (accessed on 3 February 2026).
24. Danosa, S.A. Danopren TR-P—Rigid Extruded Polystyrene Foam (XPS) for Thermal Insulation. In *Technical Sheet (in Portuguese)*; Danosa, S.A.: Pombal, Portugal, 2025. Available online: https://www.danosa.com/pt-pt/produto/danopren-tr-p/ (accessed on 3 February 2026).
25. Secil Martingança. Isovit Painel ICB—Black Cork Agglomerate Panel (FT 13016.01). In *Technical Sheet (in Portuguese)*; Secil Martingança: Lisbon, Portugal, 2019. Available online: https://www.secil.pt/pt/produtos/argamassas/sistema-etics/isovit-painel-em-aglomerado-negro-de-cortica—icb (accessed on 3 February 2026).
26. Secil Martingança. Isovit Panel EPS 100/150 (FT 13018.02). In *Technical Sheet (in Portuguese)*; Secil Martingança: Lisbon, Portugal, 2021. Available online: https://www.secil.pt/pt/produtos/argamassas/sistema-etics/isovit-painel-em-poliestireno-expandido—eps-100 (accessed on 3 February 2026).
27. Borrero-López, A.M.; Nicolas, V.; Marie, Z.; Celzard, A.; Fierro, V. A review of rigid polymeric cellular foams and their greener tannin-based alternatives. *Polymers* **2022**, *14*, 3974. [CrossRef] [PubMed]

28. *DIN 4102-1*; Fire Behaviour of Building Materials and Elements—Part 1: Building Materials; Concepts, Requirements and Tests. Deutsches Institut für Normung, Beuth Verlag: Berlin, Germany, 1998.
29. *EN 13501-1*; Fire Classification of Construction Products and Building Elements—Part 1: Classification Using Data from Reaction to Fire Tests. European Committee for Standardization: Brussels Belgium, 2018.
30. Santos, T.; Luijten, N.W.; Santos Silva, A.; Silvestre, J.D.; Faria, P. Earthen plasters hygrothermal and mechanical performance: Effect of adding recycled gypsum from plasterboards and raw hemihydrate. *J. Build. Eng.* **2024**, *98*, 111407. [CrossRef]
31. Drdácký, M.; Lesák, J.; Niedoba, K.; Valach, J. Peeling tests for assessing the cohesion and consolidation characteristics of mortar and render surfaces. *Mater. Struct.* **2015**, *48*, 1947–1963. [CrossRef]
32. *EN 12089:2013*; Thermal Insulating Products for Building Applications—Determination of Bending Behaviour. CEN: Brussels, Belgium, 2013.
33. *ISO 29469:2022*; Thermal Insulating Products for Building Applications—Determination of Compression Behaviour. International Organization for Standardization: Geneva, Switzerland, 2022.
34. *EN 1015-4:1998*; Methods of Test for Mortar for Masonry—Part 4: Determination of Consistence of Fresh Mortar (by Flow Table). CEN: Brussels, Belgium, 1998.
35. Candigrés—Ceramics Products, S.A. Candiwall® Board—Rigid Extruded Polystyrene Foam (XPS) for Thermal Insulation. In *Technical Sheet, Rev. 01*; Candigrés—Ceramics Products, S.A.: Anadia, Portugal, 2021.
36. *ISO 12572:2016*; Hygrothermal Performance of Building Materials and Products—Determination of Water Vapour Transmission Properties. International Organization for Standardization: Geneva, Switzerland, 2016.
37. Lima, J.; Faria, P.; Santos Silva, A. Earth plasters: The influence of clay mineralogy in the plasters' properties. *Int. J. Archit. Herit.* **2020**, *14*, 948–963. [CrossRef]
38. *DIN 18947:2024*; Earth Plasters—Terms and Definitions, Requirements and Test Methods. Deutsches Institut für Normung: Berlin, Germany, 2024.
39. *EN 1604:2013*; Thermal Insulating Products for Building Applications—Determination of Dimensional Stability Under Specified Temperature and Humidity Conditions. CEN: Brussels, Belgium, 2013.
40. *ISO 29767:2019*; Thermal Insulating Products for Building Applications—Determination of Short-Term Water Absorption by Partial Immersion. International Organization for Standardization: Geneva, Switzerland, 2019.
41. *ISO 15148:2002*; Hygrothermal Performance of Building Materials and Products—Determination of Water Absorption Coefficient by Partial Immersion. International Organization for Standardization: Geneva, Switzerland, 2002.
42. *EN 16322:2013*; Thermal Insulating Products for Building Applications—Determination of the Short-Term Water Absorption by Diffusion. CEN: Brussels, Belgium, 2013.
43. *ISO 11925-2:2002*; Reaction to Fire Tests—Ignitability of Building Products Subjected to Direct Impingement of Flame—Part 2: Single-Flame Source Test. International Organization for Standardization: Geneva, Switzerland, 2002.
44. *ASTM E1131-25*; Standard Test Method for Compositional Analysis by Thermogravimetry. ASTM International: West Conshohocken, PA, USA, 2025. [CrossRef]
45. *ASTM E1755-01(2015)*; Standard Test Method for Ash in Biomass. ASTM International: West Conshohocken, PA, USA, 2015. [CrossRef]
46. Vandecasteele, C.; Block, C.B. *Modern Methods for Trace Element Determination*; Wiley: Chichester, UK, 1993. [CrossRef]
47. *EN 12457:2002*; Characterisation of Waste—Leaching—Compliance Test for Leaching of Granular Waste Materials and Sludges. CEN: Brussels, Belgium, 2002.
48. Azadeh, E.; Abdullah, U.H.; Ali, N.B.M.; Pizzi, A.; Gerardin-Charbonnier, C.; Gerardin, P.; Samiun, W.S.; Ashari, S.E. Development of water repellent, non-friable tannin–furanic–fatty acids biofoams. *Polymers* **2022**, *14*, 5025. [CrossRef] [PubMed]
49. Chen, X.; Xi, X.; Pizzi, A.; Fredon, E.; Zhou, X.; Li, J.; Gerardin, C.; Du, G. Preparation and characterization of condensed tannin non-isocyanate polyurethane (NIPU) rigid foams by ambient temperature blowing. *Polymers* **2020**, *12*, 750. [CrossRef] [PubMed]
50. Eckardt, J.; Neubauer, J.; Sepperer, T.; Donato, S.; Zanetti, M.; Cefarin, N.; Vaccari, L.; Lippert, M.; Wind, M.; Schnabel, T.; et al. Synthesis and characterization of high-performing sulfur-free tannin foams. *Polymers* **2020**, *12*, 564. [CrossRef] [PubMed]
51. Eckardt, J.; Sepperer, T.; Cesprini, E.; Šket, P.; Tondi, G. Comparing condensed and hydrolysable tannins for mechanical foaming of furanic foams: Synthesis and characterization. *Molecules* **2023**, *28*, 2799. [CrossRef] [PubMed]
52. Mattos, B.D.; Zhu, Y.; Tardy, B.L.; Beaumont, M.; Ribeiro, A.C.R.; Missio, A.L.; Otoni, C.G.; Rojas, O.J. Versatile assembly of metal–phenolic network foams enabled by tannin–cellulose nanofibers. *Adv. Mater.* **2023**, *35*, 2209685. [CrossRef] [PubMed]
53. Wu, X.; Yan, W.; Zhou, Y.; Luo, L.; Yu, X.; Luo, L.; Fan, M.; Du, G.; Zhao, W. Thermal, morphological, and mechanical characteristics of sustainable tannin bio-based foams reinforced with wood cellulosic fibers. *Ind. Crops Prod.* **2021**, *158*, 113029. [CrossRef]
54. Koh, C.H.; Gauvin, F.; Schollbach, K.; Brouwers, H.J.H. Investigation of material characteristics and hygrothermal performances of different bio-based insulation composites. *Constr. Build. Mater.* **2022**, *346*, 128440. [CrossRef]
55. Kumar, D.; Alam, M.; Zou, P.X.W.; Sanjayan, J.G.; Memon, R.A. Comparative analysis of building insulation material properties and performance. *Renew. Sustain. Energy Rev.* **2020**, *131*, 110038. [CrossRef]

56. Posani, M.; Veiga, M.d.R.; de Freitas, V.P. Towards resilience and sustainability for historic buildings: A review of envelope retrofit possibilities and a discussion on hygric compatibility of thermal insulations. *Int. J. Archit. Herit.* **2021**, *15*, 807–823. [CrossRef]
57. Posani, M.; Veiga, R.; Peixoto de Freitas, V. Thermal renders for traditional and historic masonry walls: Comparative study and recommendations for hygric compatibility. *Build. Environ.* **2023**, *228*, 109737. [CrossRef]
58. Fouchal, F.; Gouny, F.; Maillard, P.; Ulmet, L.; Rossignol, S. Experimental evaluation of hydric performances of masonry walls made of earth bricks, geopolymer and wooden frame. *Build. Environ.* **2015**, *87*, 234–243. [CrossRef]
59. Cagnon, H.; Aubert, J.-E.; Coutand, M.; Magniont, C. Hygrothermal properties of earth bricks. *Energy Build.* **2014**, *80*, 208–217. [CrossRef]
60. Liuzzi, S.; Hall, M.; Stefanizzi, P.; Casey, S. Hygro-thermal behaviour and relative humidity buffering of unfired and hydrated lime-stabilised clay composites in a Mediterranean climate. *Build. Environ.* **2013**, *61*, 82–92. [CrossRef]
61. McGregor, F.; Heath, A.; Fodde, E.; Shea, A. Conditions affecting the moisture buffering measurement performed on compressed earth blocks. *Build. Environ.* **2014**, *75*, 11–18. [CrossRef]
62. Fabbri, A.; Colinart, T.; Auger, S.; Aubert, J.-E.; Faria, P.; Grillet, A.C.; Perlot, C.; McGregor, F. Recommendation of RILEM TC 274-TCE: Test method to determine the apparent water vapor transfer coefficient of earthen materials. *Mater. Struct.* **2025**, *58*, 159. [CrossRef]
63. Lima, J.; Faria, P. Eco-efficient earthen plasters: The influence of the addition of natural fibers. In *Natural Fibres: Advances in Science and Technology Towards Industrial Applications*; RILEM Bookseries; Fangueiro, R., Rana, S., Eds.; Springer: Dordrecht, The Netherlands, 2016; Volume 12, pp. 315–327. [CrossRef]
64. Lima, J.; Faria, P.; Santos Silva, A. Earthen plasters based on illitic soils from Barrocal region of Algarve: Contributions for building performance and sustainability. *Key Eng. Mater.* **2016**, *678*, 64–77. [CrossRef]
65. Ranesi, A.; Faria, P.; Veiga, M.R. Traditional and modern plasters for built heritage: Suitability and contribution for passive relative humidity regulation. *Heritage* **2021**, *4*, 2337–2355. [CrossRef]
66. *DIN 4108-3:2018*; Thermal Protection and Energy Economy in Buildings—Part 3: Protection Against Moisture Subject to Climate Conditions—Requirements, Calculation Methods and Directions for Planning and Construction. Deutsches Institut für Normung: Berlin, Germany, 2018.
67. Celzard, A.; Fierro, V.; Amaral-Labat, G.; Pizzi, A.; Torero, J. Flammability assessment of tannin-based cellular materials. *Polym. Degrad. Stab.* **2011**, *96*, 477–482. [CrossRef]
68. Lim, S.Y.; Park, S.B.; Kim, M.S.; Kim, J.H.; Lee, H.J.; Choi, S.H. Study on the mechanical properties and flame retardancy of tannic acid-based non-isocyanate rigid polyurethane foam according to the content of crosslinking agents. *Adv. Ind. Eng. Chem.* **2025**, *1*, 15. [CrossRef]
69. DSouza, A.; Dodangeh, F.; Balaji Venkata, G.; Ray, M.B.; Prakash, A.; Xu, C. A comprehensive review of biobased polyurethane and phenol formaldehyde hydrophilic foams for environmental remediation, floral, and hydroponics applications. *Biomass Bioenergy* **2025**, *192*, 107493. [CrossRef]
70. Paciorek-Sadowska, J.; Borowicz, M.; Isbrandt, M.; Czupryński, B.; Apiecionek, Ł. The use of waste from the production of rapeseed oil for obtaining of new polyurethane composites. *Polymers* **2019**, *11*, 1431. [CrossRef] [PubMed]


**Disclaimer/Publisher's Note:** The statements, opinions and data contained in all publications are solely those of the individual author(s) and contributor(s) and not of MDPI and/or the editor(s). MDPI and/or the editor(s) disclaim responsibility for any injury to people or property resulting from any ideas, methods, instructions or products referred to in the content.